Analysis of faults and pit chains in Noctis Labyrinthus: Implications for early extension and possible magmatic plumbing

Mayssa El Yazidi[1,2], Csilla Orgel[1], Elliot Sefton-Nash[1], Guido De Marchi[1], Bahia Rickbir [1], David Baratoux[3,4], Sylvain Bouley,[5,6] Justin Filiberto[7], Piero D'Incecco[8,9], Giovanni Leone[10], Slim Shimi Najet[11], Feyda Srarfi[11], Balázs Bradák[12]

[1]ESTEC - European Space Agency, The Netherlands; [2]Center for Studies and Activities for Space - CISAS, University of Padova, Italy; [3] Géosciences Environnement Toulouse, CNRS, UPS & IRD, Toulouse, France; [4]UFR des Sciences de la Terrre et des Ressources Minières, Université Félix Houphouët-Boigny, Abidjan Cocody, Côte d'Ivoire; [5]Université Paris-Saclay, CNRS, GEOPS, 91405 Orsay, France; [6]IMCCE, Observatoire de Paris, France; [7]Astromaterials Research and Exploration Science (ARES) Division, NASA Johnson Space Center, Houston, TX, 77058, USA; [8]National Institute for Astrophysics (INAF) - Astronomical Observatory of Abruzzo, Teramo, Italy; [9]Arctic Planetary Science Institute (APSI), Rovaniemi, Finland; [10]Instituto de Investigaciónen Astronomía y Ciencias Planetarias, Universidad de Atacama, Copiapó, Chile; [11]Faculty of Sciences of Tunis, University of Tunis El Manar, Tunisia; [12]Laboratory of Exo-Oceans, Faculty of Oceanology, Kobe University, Japan.

Abstract

Noctis Labyrinthus has been a region of disputed origin due to its complexity and poor understanding of how various processes and mechanisms may have combined to form it. The surface is an integrated record of intensive tectonic activity expressed by a multiple extended sets of dip-slip faults oriented in different directions, and thought to have acted on this region over its history. These faults are always coalescent to pits and pit chains displaying a complicated geological history in the region. To understand this geological history, we mapped the surface features in Noctis Labyrinthus using the High-Resolution Stereo Camera (HRSC) onboard Mars Express ND2 nadir channel basemaps, and we adapted the Digital Terrain Map (DTM) from the Mission Experiment Gridded Data Record (MEGDR) of Mars Orbiter Laser Altimeter (MOLA) onboard Mars Global Surveyor (MGS) for the topography. We have investigated the spatial distribution and trend of fault systems, the pit chains' morphology, and the correlation between these two types of features. Our results show three fault systems: i) NS and NNE-SSW, ii) EW and ENE-WSW, and iii) NNW-SSE and NW. The analysis of the faults trending, cross-cutting correlation and the superimposition led to identify multiple intersections between these faults that have been alongside with the reactivations of some inherited faults. We interpreted the first system of fault to be related to coeval lateral extension, generated by regional stress tensor, which is probably related to the slight bending of Valles Marineris within two phases of bidirectional extension. The second system of faults has been generated by the radial oblate stress tensor related to the formation of the small shield volcanoes in Syria Planum. However, the third system is likely related to the external driving process, probably in the Tharsis province. We classified pits in four evolutionary stages based on their morphometric attributes. We believe that the formation of the pit chains in Noctis Labyrinthus is related to a surface collapse after a pressure drop related to the magma chamber deflation associated with Syria Planum volcanic province. We propose a deformational model based on early extension and magmatic plumbing as driving processes for the formation of Noctis Labyrinthus.

1. Introduction

Noctis Labyrinthus connects some of the most significant topographic features on the surface of Mars. It spans ~882 km east to west, and ~393 km north to south, bordered to the east by Valles Marineris, to the west by the vast volcanic plateau of Tharsis, and to the south by the lava plains of Syria Planum divide [Fig.1]. Valles Marineris is the largest canyon on Mars (Lucchitta et al., 1992; Lucchitta et al., 1994), thought to involve a combination of horizontal extension and vertical subsidence or lateral collapse (Carr., 1974; Masson.,1985; Schultz., 1989; Schultz., 1999; Dohm et al., 2009; Mège & Bourgeois., 2011; Andrews-

Hanna., 2012a,b; Brustel et al., 2017). Several extensional fault systems have been identified in Valles Marineris and considered to be related to the evolution of several tectonic centers in the region (Anderson et al., 2001) developing from the Noachian to the Amazonian (Richardson et al., 2013). To the northwest of Valles Marineris sits off the Tharsis region. The volcanic plateau of Tharsis hosted essentially most of the volcanic activity on Mars, and covers nearly a quarter of the planet's surface (Greeley & Spudis., 1981; Head et al., 2002; Johnson & Phillips., 2005; Baker et al., 2007; Dohm et al., 2007; Hauber et al., 2011; Yin, 2012; Beuthe et al., 2012, Leone., 2021; Leone et al., 2022). The volcano-tectonic activity of Tharsis was estimated to start in Late-Noachian (Bouley et al., 2018), but a possible Pre-Noachian activity cannot be excluded (Leone et al., 2022).

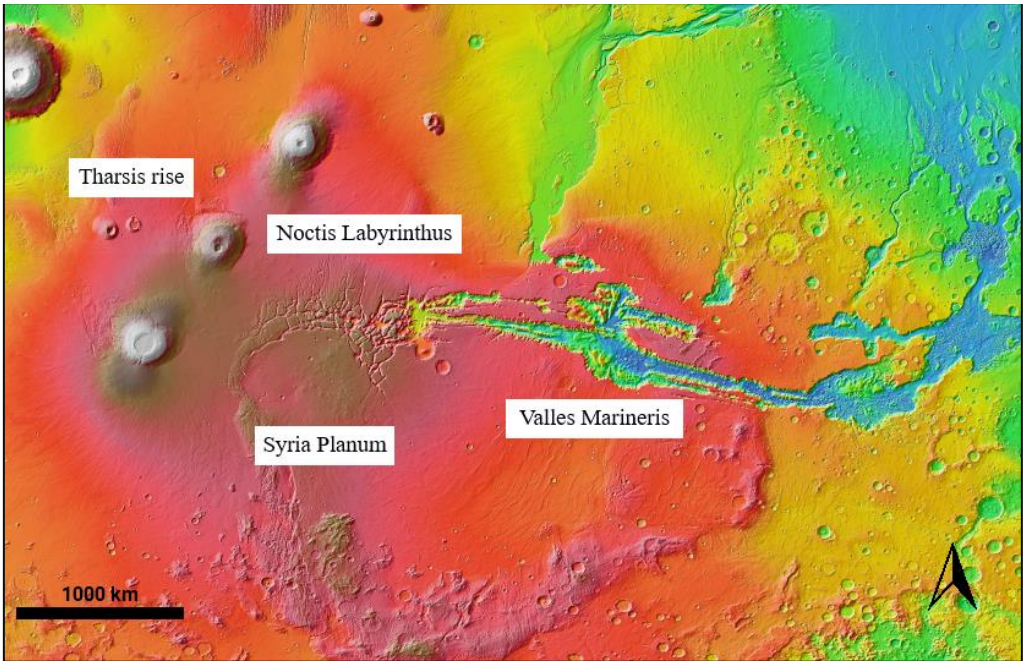

Figure 1. Noctis Labyrinthus topographic context and the main geologic features in the surrounding area. The region between Noctis Labyrinthus and Syria Planum have been identified as an extensional zone. In the East of Noctis Labyrinthus is located the Valles Marineris shear zone, where major groups of extensional faults have been documented. View centered at -6.625°N_260,625°E.

To the southeast of the Tharsis region, there is the broad plateau of Syria Planum, bordered by Noctis Labyrinthus to the north and Solis Planum to the southeast. Syria Planum is punctuated by small volcanic edifices and extensive volcanic landforms (Richardson et al., 2013) that have been several times called as the most prominent features for a magmatic-driven activity identified in the Tharsis bulge (Anderson et al., 2004; Yin., 2012; Pozzobon et al., 2021,2023). Previous studies from Anderson et al., 2004 suggested that the magmatic activity of Syria Planum was related to an episode of intense tectonism (Tanaka & Davis., 1988) during the Late-Noachian to the Early-Hesperian. Furthermore, Mège & Masson., 1996 proposed a radial extension of Syria Planum controlling the Valles Marineris formation.

The emplacement related activity for the Tharsis province, Valles Marineris and Syria Planum are clearly associated with intense volcanic and tectonic activities, observed certainly with stratigraphic relationship at the surface, and must have participated in the formation of Noctis Labyrinthus.

Noctis Labyrinthus displays intriguing surface geomorphology, characterized by inter-connected sets of extensional fault systems and grabens, manifest in numerous orientations with different dimensions and trends. By extension, these faults are often correlated to scalloped pits and pit chains, predominantly developing along the same strike for tens of kilometres scale, parallel or colinear, creating a coalescent

complex feature of unknow origin. The formation of Noctis Labyrinthus remains ambiguous and a topic of substantial discussions, although it is widely thought to involve a combination of two or more processes. Earlier work from Weitz & Bishop., 2014, identified several periods of aqueous activity and alteration occurred within troughs in Noctis Labyrinthus, led to support recent interpretations about a potential karst landscape with associated caves and water-related processes. Rodriguez et al., 2016 proposed a structurally-controlled groundwater flow through salt-rich upper crustal deposits as a driving process for the complex surface features in Noctis Labyrinthus. By extension, Baioni et al., 2017, Baioni,.2018suggested an evaporite karst landforms with associated caves and water-related process, Chavan et al.,2022 defined fluvial process based on structural mapping and surface interpretation. Alternatively, Leone., 2014 argue an erosional evolution that leads to fossae after the collapse of the lava tubes, while Kling et al., 2021 suggested a tectonic deformation and volatile loss in Noctis Labyrinthus. Several other hypotheses acknowledged a volcanic and tectonic activity by Masson., 1977; Mège & Masson., 1996; Schultz., 1998; Mège et al., 2003;Bistachi et al., 2004; El Yazidi et al., 2023.Although these various hypothesis, none of the proposed formation models have been widely accepted, which implies that Noctis Labyrinthus indeed deserves further consideration, observations, and new approaches of study.

Previous research from Mège & Masson.,1996; Baptista et al., 2008; Schultz., 1998; Mège et al., 2003; Kling et al., 2021; Pozzobon et al., 2021, 2023, documented several crosscutting and intersecting fault systems, extended over Noctis Labyrinthus, creating extensional structures likely associated to several tectonic phases. A thorough study of these fault sets will offer answers about the tectonic setting, phases, and the related events, toidentify the sequence of the deformational events that lead to the formation of Noctis Labyrinthus. The age of these fault systems and the related tectonic phases in Noctis Labyrinthus remains uncertain. Further, some fault systems seem to be reactivated several times after their inception, displaying a complex tectonic history (El Yazidi., 2023). Schultz.,1998 argued three deformational stages for Valles Marineris in which Noctis Labyrinthus is involved: first stage of radial dike emplacement in Syria Planum during Late-Noachian to Early-Hesperian, second stage characterized by localized crustal subsidence of Post-Hesperian to Early-Hesperian, and a third stage of regional normal faulting, which controlled the formation of troughs in Noctis Labyrinthus and Valles Marineris, during the Amazonian period. Bistacchi et al., 2004 instead proposed two deformational phases in Noctis Labyrinthus based on the faults cross-cutting relationships and analysis of surface structures: The first tectonic event belongs to the Noachian, mainly expressed in the north, described by transtensional faults, several of them are mostly oriented NNE. However, more minor faults trending NS and WNW were interpreted as a conjugate structure. The second tectonic event is documented on the southern side of the Noctis Labyrinthus, represented by an extensional fault system along NNE–SSW, and WNW-ESE trends, likely related to Valles Marineris formation and they are Late-Noachian to Early-Hesperian aged. The NNE-SSW extension is muddled by pre-existing structures from the first deformational phase. The WNW trending grabens are larger than those in the NNE, indicating a relative dip-displacement along the WNW fault set. Further, Bistacchi et al., 2004 suggested a third event to be dextral NW strike-slip faults, cross-cutting Valles Marineris, and may belong to the Late-Hesperian.

The objective of this manuscript is to provide a new insight into the formation of Noctis Labyrinthus through a detailed structural and geomorphological analysis. For this purpose, we produced a structural map of the selected region in Noctis Labyrinthus. This map will allow us to study the fault systems, kinematics, quantification of displacement and chronological relationships between fault systems to determine the sequence of tectonic phases related to those fault systems. The fault systems and tectonic phases likely to be overestimated in previous studies (Masson.,1977; Mège & Masson., 1996; Schultz, (1998); Mège et al., 2003;Bistachi et al., 2004; Rodriguez et a., 2016; Baioni et al., 2017, Baioni, (2018); Kling et al., 2021;Chavan et al., 2022) due to the inability to resolve and characterize these intersections

and fault properties in lower resolution datasets, or the overmapping of some surface features. Pit chains are also considered to be an important aspect of the development of Noctis Labyrinthus and their formation seems to be related to the spatial distribution of the faults' intensity. We also aim here to provide a detailed analysis of the fault systems and pits, and the relationship between these features. We will test and further various hypotheses for the formation of Noctis Labyrinthus from geomorphologic and structural perspectives. We will execute a detailed structural map that will allow enhancements for the study of the fault systems, tectonic phases, pits evolutionary stages and the clustering of faults-graben-pits system radiating from shear zone.

2. Data and Methods

2.1. Data sets

A few maps have been realized for Noctis Labyrinthus, some of these maps display only faults and grabens distribution (Masson., 1977; Mège et al., 2003; Bistacchi et al., 2004; Montgomery et al., 2009), other maps shows more details of the surface features like troughs, landslides and pit craters (Rodriguez et al., 2016; Baioni et al., 2017; Kling et al., 2021), or geologic maps that were delivered with age assignments of lithologic units (Scott & Tanaka., 1986). The scope of this study area extends over h3210_0000 and h3221_0000 orthoimages from the High-Resolution Stereo Camera (HRSC) onboard Mars Express. The research area that will be explored in this work has been selected based on the data availability and the interesting connection between the surface features, to study in detail the surface geomorphology in Noctis Labyrinthus and address the gaps in previous works.

To produce the map for the study area, we opted to generate a complete monochrome mosaic made by h3210_0000 and h3221_0000 orthoimages, from ND2 nadir channel [Fig.2].These orthoimages are calibrated data from the MEX HRSC Version 3 Reduced Data Record (RDRV3) bearing an average resolution of ~19.5 m/pixel. For the topography, we used the MEGT00N180HB derived data from the Mission Experiment Gridded Data Record (MEGDR) of Mars Orbiter Laser Altimeter (MOLA) onboard Mars Global Surveyor (MGS), bearing a resolution of 463m/pixel to determine the maximum vertical displacement (D_{Max}) [Fig.2]. We used the context Camera (CTX) dataset from Mars Reconnaissance Orbiter (MRO), bearing a resolution of 5.2m/pixel [Tab.1] for small-scale analysis of some surface features like hummocky deposits, pits and pit chains floors, and shaped faults intersections. The data resolution was sufficient for the mapping, analysing the faults spatial distribution, studying the pits morphometric attributes, and delivering a high-resolution map of Noctis Labyrinthus. The uncontrolled nature of the mosaic didn't affect the mapping results in this study.

Table 1. MRO CTX Experiment Data Record (EDR) images mosaic

CTX Image ID	Map resolution	Incidence Angle	Emission Angle
B01_010160_1757_XI_04S104W	5.56 mpp	58.75	12.62
B11_014063_1737_XN_06S103W	5.26 mpp	36.41	0.95
G02_019087_1727_XN_07S103W	5.53 mpp	57.53	18.04
J01_045170_1728_XI_07S103W	5.24 mpp	54.58	3.29
J02_045513_1744_XI_05S104W	6.11 mpp	54.47	22.35
J05_046937_1735_XN_06S104W	5.28 mpp	51.82	4.55
J11_049218_1737_XI_06S102W	5.6 mpp	34.96	14.67

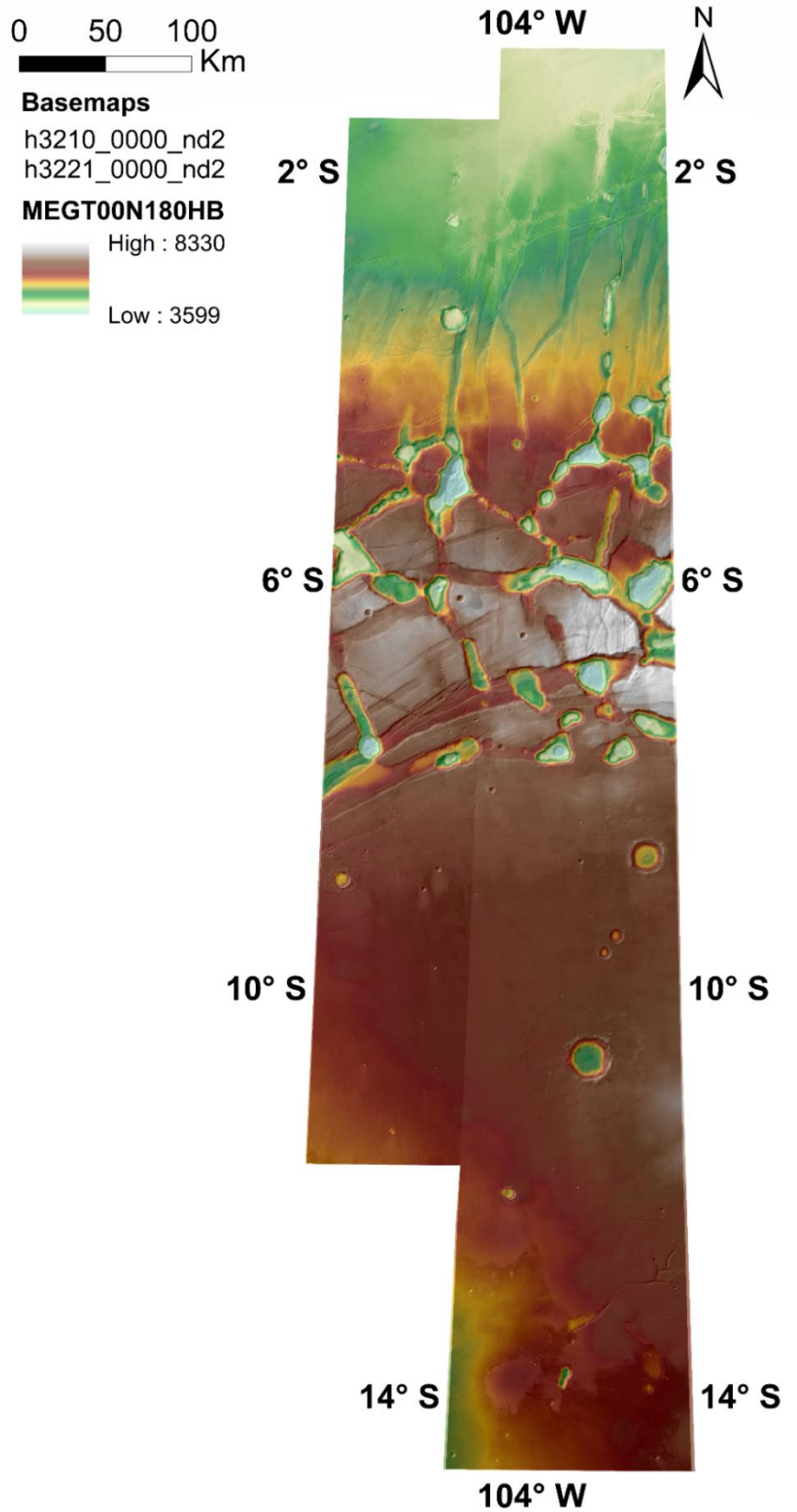

Figure 2. HRSC basemaps overlay the studied area's MOLA DEM MEGT00N180HB topographic dataset. Data projected in Equirectangular Mars. Image centered at 104.28°W_5.68°S.

2.2. Methods

To avoid the over-mapping and the pixelation of some features that might affect the surface properties during the mapping and the final map, we followed the recommendation of Tobler (1987) for the mapping and output guidelines. Given the basemap resolution, the digitization scale is 2,000 × the basemap raster resolution. Thus, the mapping scale should be no smaller than 1:39,000. We mapped all features in full-featured Geographic Information System (GIS) application ArcGIS 10.7.1 from Esri software packages. The data is projected in equirectangular projection, centered between the 102 and 104 West meridians, to minimize distortion across the entire length of the strip. To examine the fault spatial distribution, pits and pit chains characteristics, and investigate the relationship between these features, we applied the following methodology for the mapping.

2.2.1. Mapping of faults

We classified faults and grabens as linear features; thus, they were mapped by a polyline shapefile in continuous simple, bold lines. We divided faults in two main classes based on their length. Major faults are described by a length ≥ 4km, and minor faults are < 4km of length. This classification was based on the global intensity of the faults' distribution according to their size. To avoid the overload and surcharge of the mapped features, we maintained only these two classes of faults.

Considering that the area is intensively tectonized, faults frequently crosscut and consequently they were divided into several segments. The mapping of faults includes branching, segmented, ramping, and single isolated faults. Each fault was traced by a single polyline, except for the segmented faults, mapped by a group of individual polylines. The minor faults are mostly displayed on single lineament; thus, their length was derived from the polyline length. The total length of the segmented faults, that was almost entirely major faults, have been derived by the sum of the polylines' length who delineate the mapped fault segments. Some faults were difficult to track, or their extension and length were uncertain likely to the basemaps resolution, so they were not mapped in this work.

2.2.2. Mapping of pits and pit chains

Pits and pit chains show oval-shaped and elongated depressional forms, flat-floored and linearly aligned along the graben. To determine the pits and pit chains dispersion, dimension and interconnection, we symbolized their full shape by a polygon shapefile as illustrated in Figure 3. a. To determine the orientation of pits and pit chains, we mapped their rim by continuous simple bold lines alongside their lengths [Fig.3.b]. The azimuth dispersion was derived from the polylines by the polylines' length. The mapping includes aligned pits, single isolated pits, and pit chains. The steep-sided edge of the pit chains helped for tracking their trends and linework [Fig.3.b], to analyse their spatial distribution and orientation relatively to faults and grabens. The major part of these pits is robustly connected to each other, coalescing, merging, or sharing boundaries, and consequently, they were mapped as a merged unit. The single isolated pits were mapped as individual unit. Some of the pits displayed hummocky deposit within their floor, these deposits were mapped by a specific polygon shapefile.

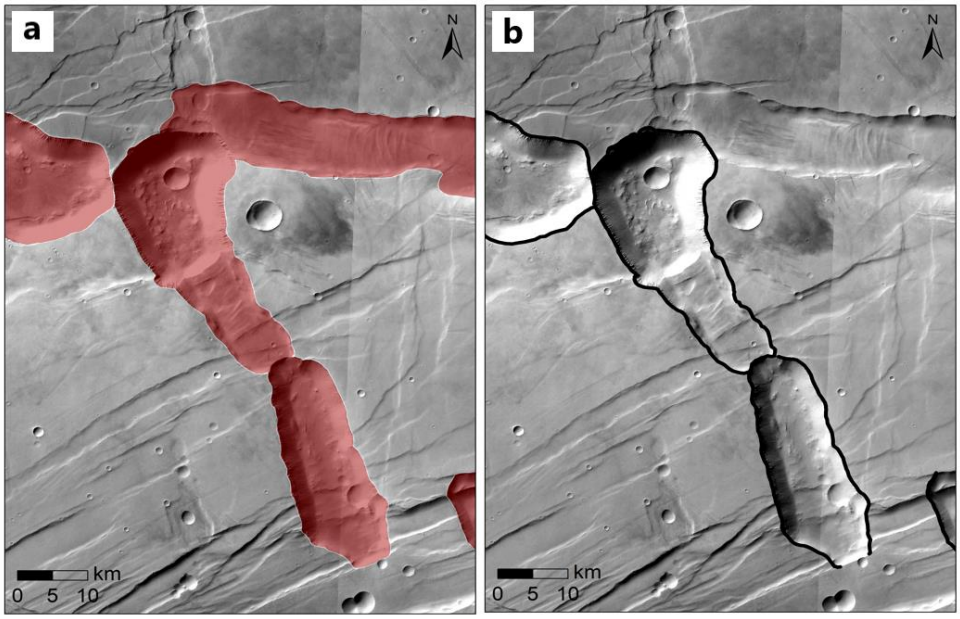

Figure 3. Pit chains mapping approach (a) Mapping of the pit chains edge by a polyline shapefile (b) Pit chains full shape mapping using a polygon shapefile. View centered at -6,461°N_255,281°E, over HRSC basemap.

To distinguish extended graben with important subsidence from aligned merged pits, we applied the following criteria based on geometrical and morphometric attributes of these two types of features:

1) *Lack of curvature*: A graben tends to ignore topography and generally forms linear features (i.e., straight) while pit chains can have a more sinuous and rounded appearance due to pre-existing topography.

2) *Length*: Grabens due to local tectonics might be short compared to the pit chains that extend as far as pits are merged by eroding pre-existing topography.

3) *Width*: Grabens generally have narrow widths, while pits and pit chains increase their widths due to progressive erosion and collapse of the pre-existing topography.

4) *Vertical displacement* (D_{Max}): Pits and pit chains display significant vertical displacement between the sides, that is not seen in grabens due to the important subsidence of the surface related to the pits and pit chains formation. We measured the vertical displacement for graben and pit chains using a cross-section profile over MOLA topographic data [Fig.4] to value the difference on this vertical subsidence for both types of features.

The significant length, width, vertical displacement and the curvature shape of pits and pit chains, shows that they aren't only tectonic in origin. These criteria were used as arguments to support our observations for the magmatic origin of the pits and pit chains formation.

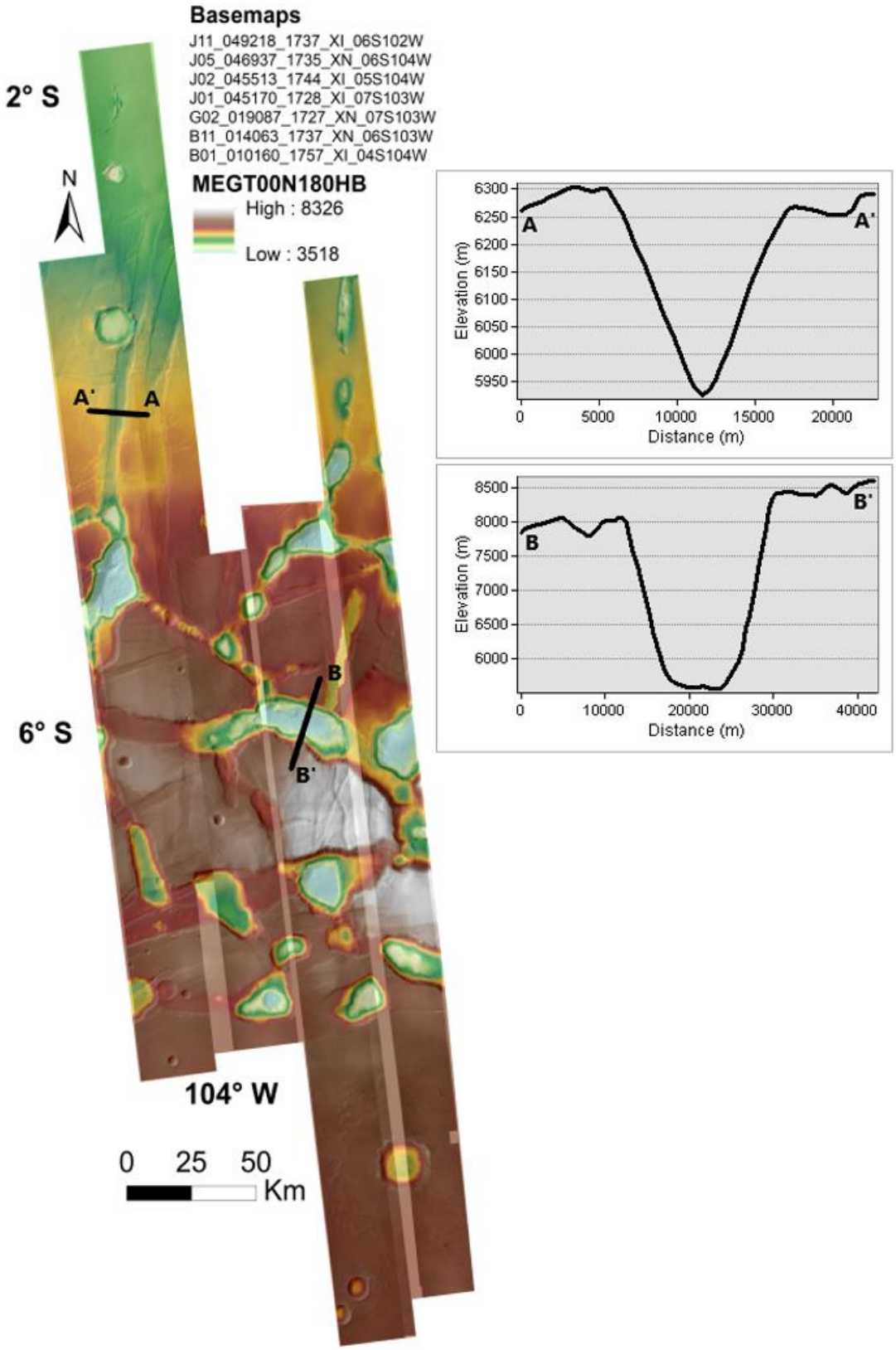

Figure 4. Cross-section profile over CTX monochrome basemaps and MOLA topographic datum, demonstrating the difference in the vertical displacement D_{Max} and curvature for graben and pit chain. (a)The section aa' is performed for a graben in the north district. The vertical displacement in the diagram is about ~350 to 400 m. (b) The bb' profile section has

been realized for the pit chain in the south. The vertical throw in the diagram shows a measurement (~2050 m) compared to graben.

3. Results

3.1. Structural map

The most recent detailed map for Noctis Labyrinthus was made at 1:200,000 mapping scale (Kling et al., 2021) using a combination of data from the Thermal Emission Imaging System (THEMIS) on 2001 Mars Odyssey' Global Day-IR mosaic at 100m/px, with CTX (6 m/px) and HRSC (~ 20–100 m/px) images when higher resolution was required for satisfactory mapping. This study will, for the first time, execute a detailed structural map for Noctis Labyrintus at 1:39,000 mapping scale, nearly a 5x resolution increase.

The higher resolution structural map that we produced is displayed in the Figure 5 using HRSC dataset. This map shows a widespread distribution of major and minor faults and grabens in the study area. A recognizable difference in the faults' intensity distribution is observed between the north and south districts. Faults became more intense, branched, segmented and increased the azimuth dispersion in the south. In the north, faults are NS, NNE-SSW, and ENE-WSW trending, parallel and/or crosscutting, generating a large branched network of intersecting grabens and series of rectangular blocks. These rectangular blocks are due to pre-existing topography and faults and serve as a record of ancient extension that shaped this region.

The faults in the northernmost are generally extended for a long distance compared to those faults of the south. The intensity of the fault distribution in the south is important compared to the north, particularly mentioning the stress shear zones, where pits and pit chains are clustering. The azimuth dispersion for the faults and grabens in the south is more evident and diffuse compared to the north. Most minor faults with lengths < 4 km are expressed in the south, robustly connected to pits and pit chains in different directions.

The major faults we mapped in the studied area are normal faults, characterized by a length > 4 km, with minor contribution of some strike-slip faults. Some of the faults we studied are continuous, even after intersection with other faults, whereas others were segmented in a group of small faults that belong to the same original fault. We derived the azimuth dispersion for major and minor faults in polar plots [Fig. 5] to determine their different orientations and identify the fault systems.

Some irregular wrinkle ridges with curved, circular or en-échelon shapes, slightly distributed in the map, repeatedly observed in higher tectonized and deformed zones or alternatively within the floor of pits and pit chains. The structural map we produced includes also the global distribution of the hummocky materials and the different evolutionary stages of the pits, which we will discuss in details within the section 3.2.

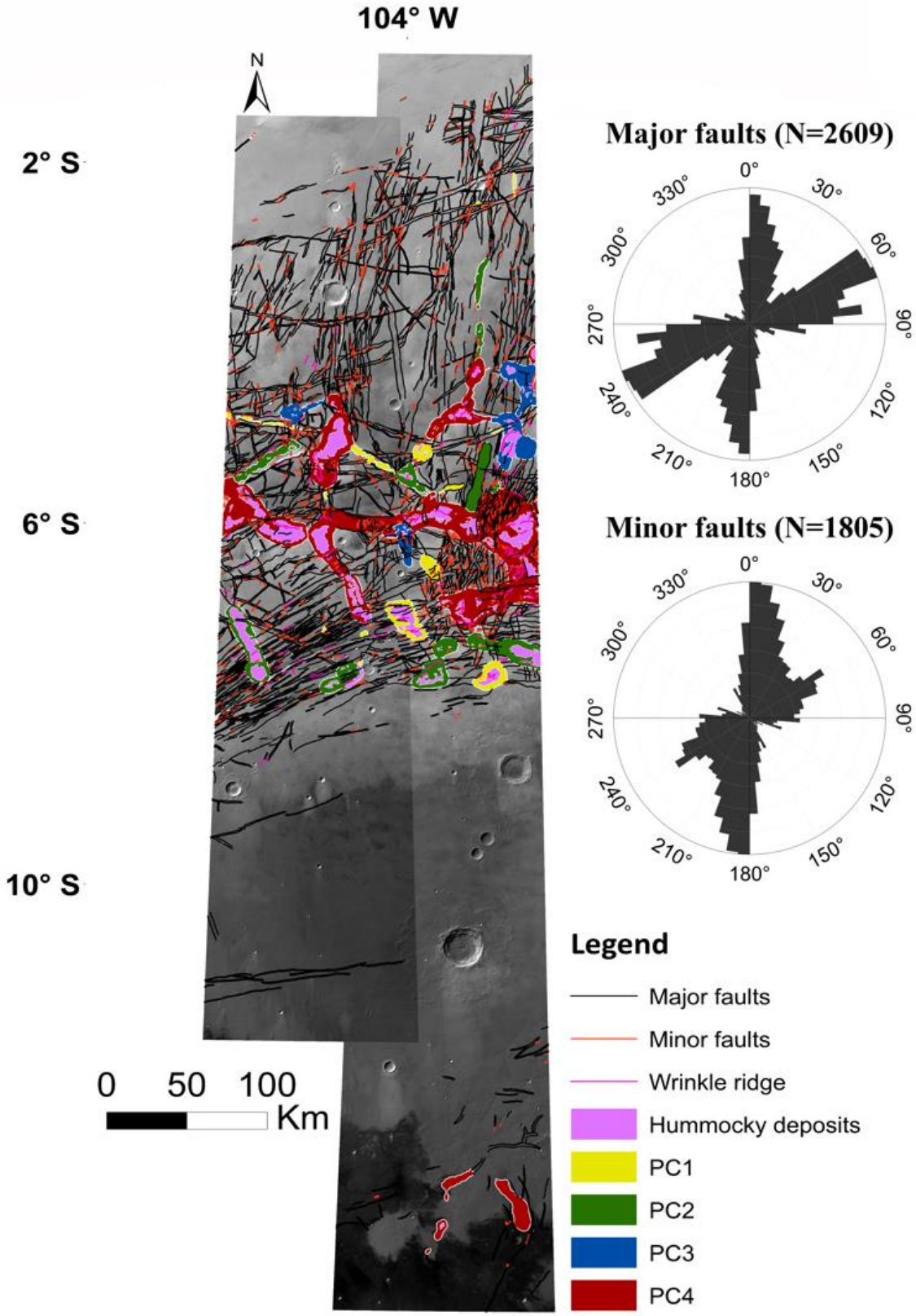

Figure 5. Noctis Labyrinthus structural Map at 1:39,000 mapping scale. The polar plots indicate the trends for major and minor faults classes. The number of faults for each class is labelled in the figure. PC1, PC2, PC3 and PC4 are respectively the 1st, 2nd, 3rd and 4th stages for the pits' formation. Features classes are labelled on the legend. Map production was through HRSC basemap, in ESRI ArcMap 10.7.1 and completed in Inkscape 0.92.4.

3.2. Global distribution of fault systems and chronology

We mapped a total of 4414 faults, including 2609 major faults, bearing a length ranging between 40 km and 74.70 km, and 1805 minor faults of length ranging between 3.9 km and 255 m. These faults are displayed over the studied area, many of them are essentially clustering within pits and pit chain areas. The difference within the faults' spatial distribution between the north and the south districts comprises the faults trending, length, and intensity. In the north, a major group of NS, NNE-SSW faults are widely displayed, with secondary contribution of ENE-WSW faults. The ENE-WSW faults became more frequent by approaching the pit chains areas, and they start to dominate the global spatial distribution of faults in the south.

We analysed the faults' trending, superimposition and cross-cutting relationship to identify the fault systems and the related tectonic phase(s). A fault is considered more recent than the fault it cuts and older than the one that cuts it. By extension, we used the standard geological approaches (Childs et al., 1995) for the relative chronology of faults and also pit chains (i.e., Principle of superposition, Principle of intersection and Principle of recovery). Based on these approaches, data extraction and positioning, we were able to identify three fault systems as demonstrated in the Figure 6. The first system (N=1792) contains faults mainly oriented in NS and NNE-SSW. These faults are often present in the northernmost, characterized by a length ranging between 0.427 km and 70.532 km and slightly fading out by getting close to pit chains areas on the south. The second system (N=1759) includes faults trending in the EW and ENE-WSW. Unlike the first system, these faults are intensely present in the south, in strict conjunction to pits and pit chains, parallel and sometime cross-cutting. Many of these faults are identified by relatively short length (0.372 km <Length<74.706 km) compared to the fault in the north due to multiple cross-cut by and with other faults. The third fault system (N=749) we identified is mainly oriented in NNW-SSE, NW-SE, and WNW-ESE strikes. Some of these faults extend for tens of kilometres (0.598 km< Length< 73 km) and are frequently interconnected with pits and pit chains.

The investigation of the different intersections between the fault systems led to interpret that NS and NNE-SSW faults are older compared to EW, ENE-WSW, NNW-SSE, NW-SE, and WNW-ESE faults. The NS and NNE-SSW faults are often overlapped and superimposed by other faults from the second and third fault systems, suggesting that the faults from the first system are generated by early extensional tectonic responsible for their formation. The second system is oriented in the ENE-WSW and EW. Faults from this system are remarkably displayed in concentric pattern, in clustering pits and pit chains areas. A large group of these faults begins from the southwest as ENE-WSW sets and progressively assumes EW strikes towards the east side, creating an arcuate swarm of concentric shaped faults and graben, arcuated towards Syria planum. These concentric shaped faults dominate the global spatial distribution of faults in the south, and they seem to have a different driving process based on their spatial distribution, trend and correlation to pits and pit chains. At the end, this system is most recently active than the fault generally produced with the first system.

Although the first fault system seems to be older compared to the second, we documented some faults from the NS and NNE-SSW trends are cut by faults from the second system, and these faults from the second system are cut afterward by the same NS and NNE-SSW faults from the first system, and vice-versa [Fig.7]. This observation demonstrates that faults holding a dual behaviour, that could eventually be related to substantial reactivation essentially occurred between inherited faults from the first and the second systems.

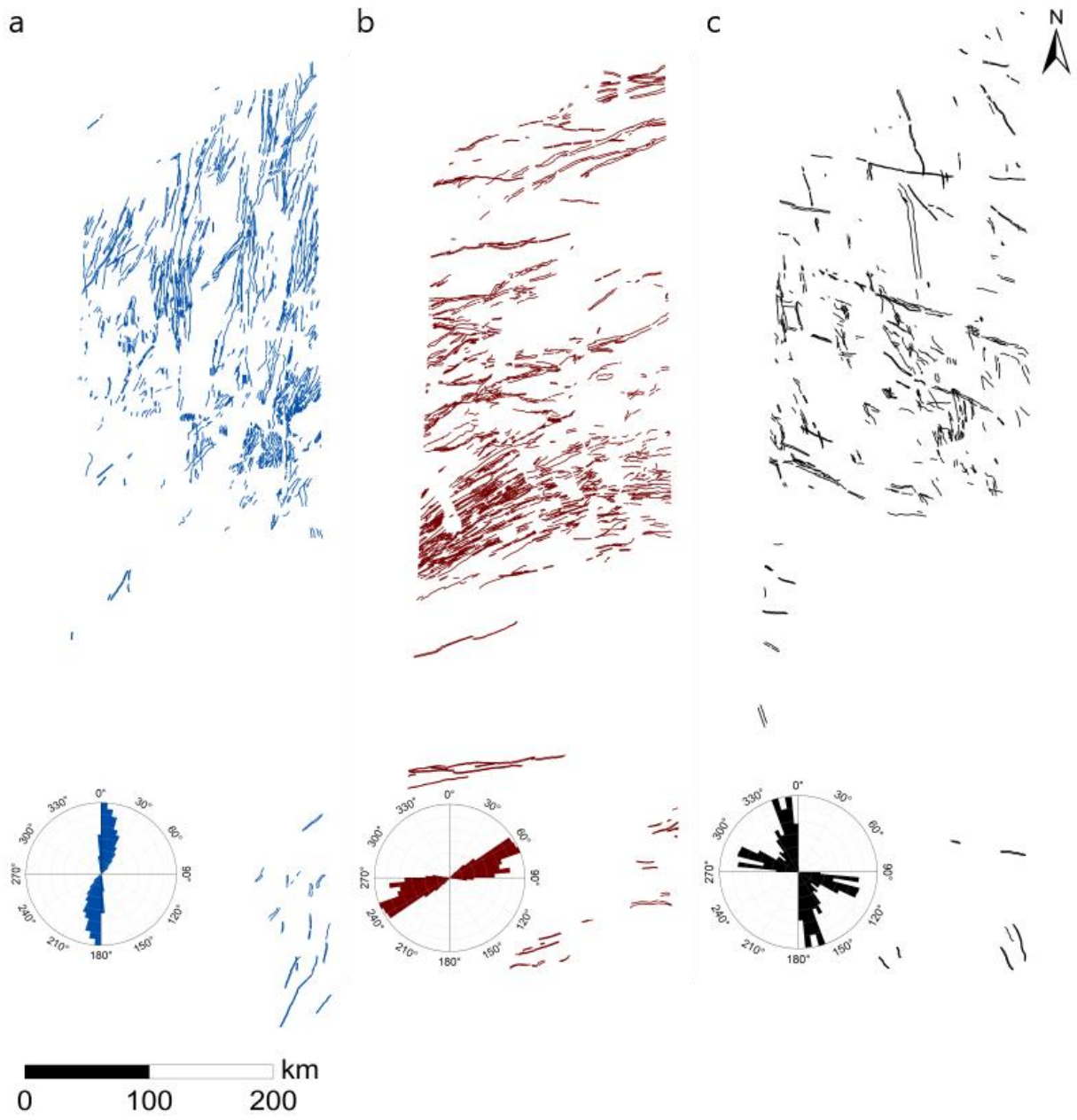

Figure 6. Global spatial faults distribution background and orientations of the three fault systems (a) First system (Blue lines) oriented NS, NNE-SSW (b) Second system (Dark umber lines) trending ENE-WSW and EW. (c) Third system (Dark lines) oriented NNW-SSE, NW-SE, and WNW-ESE. The faults mapping was realized over HRSC basemaps, the polar plots was derived from polylines by polylines' length.

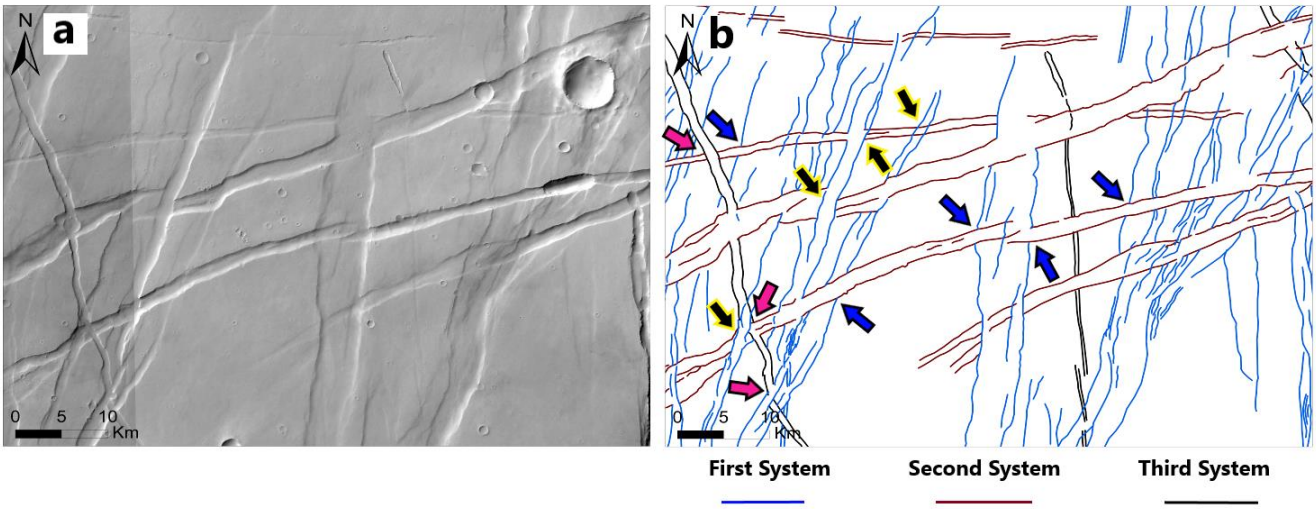

Figure 7. A close-up view for cross-cutting faults. (a) View over HRSC basemaps for the faults crosscutting relationship (b) Background interpretation shows the three fault systems. The NS and NNE-SSW faults (Red lines) are superimposed by EW and ENE-WSW faults (Green lines). The intersection spot between the first and second fault system (Blue arrow) indicates that faults from the first system are older compared to those from the second system based on their crosscutting relationship. Near these intersection districts and contrasting the previous observation, the same faults from the first system superimpose the same faults from the second system (Black arrow spot). These observations have also been identified within some faults from the third system, where NW-SE faults overlap NNE-SSW faults, later the same NW-SE faults are overlapped by the same NNE-SSW (Ginger pink arrow spot).

The third fault system contains faults mainly oriented in the NNW-SSE, NW-SE, and NW-SE. This system seems to be posterior to the previous fault systems, since its mostly cuts and superimposes NS, NNE-SSW, EW and ENE-WSW faults, and infrequent pits and pit chains. Although they are the youngest estimated in terms of chronology, few of them have also been involved in the faults reactivation observed between the first and second systems [Fig. 6].

A group of EW faults is crosscutting with other faults from the ENE-WSW in the north, generating a series of long prominent grabens, which appears as a rectangular faulted block [Fig. 6]. The azimuth dispersion for the faults and grabens in the south is more evident and diffuse than in the north. The NW-SE trending fault is much more frequent in the south than the north and is essentially connected to pit chains.

The wide network of dip-slip fault sets in the study area is generated by an important extensional tectonic strain. Alongside these dip-slip faults, some strike-slip faults with normal and transtensional kinematics have been identified with different horizontal displacement; right and left lateral motions within the NE-SW and EW trends. These internal features of crustal deformation terminate by splaying or bending. The strike-slip faults create a pull-apart structure of relatively small dimension ~ 2km length [Fig.8.a], driven by the mechanism of local extension between two en-echelon strike-slip fault segments (Aydin et al., 1990). Furthermore, a right steeping echelon segments has been documented [Fig.8.b.c], displayed as segmented and relay ramping faults that have not yet interacted significantly with each other or branching faults in between the hanging and footwall. These sets of parallel echelon arrays, grow with a consistent sense of step and are arranged as a left-stepping configuration (Peacock & Sanderson., 1991; Brent & Cartwright., 1996; Soliva et al., 2006). Some of these echelon arrays appear to be growing at low discontinuity densities and, at progressively increasing amounts of remote strain, begin to interact mechanically with adjoining discontinuities. The strike-slip faults that have been documented are formed in an extensional context and characteristically segmented, especially in their earlier stages of development. The Figure 8.b and 8.c present an example of en-echelon of parallel segmented faults in

the north, within dextral system, with geometric irregularities of the stepovers. The near-tip stress of these segments is antisymmetric.

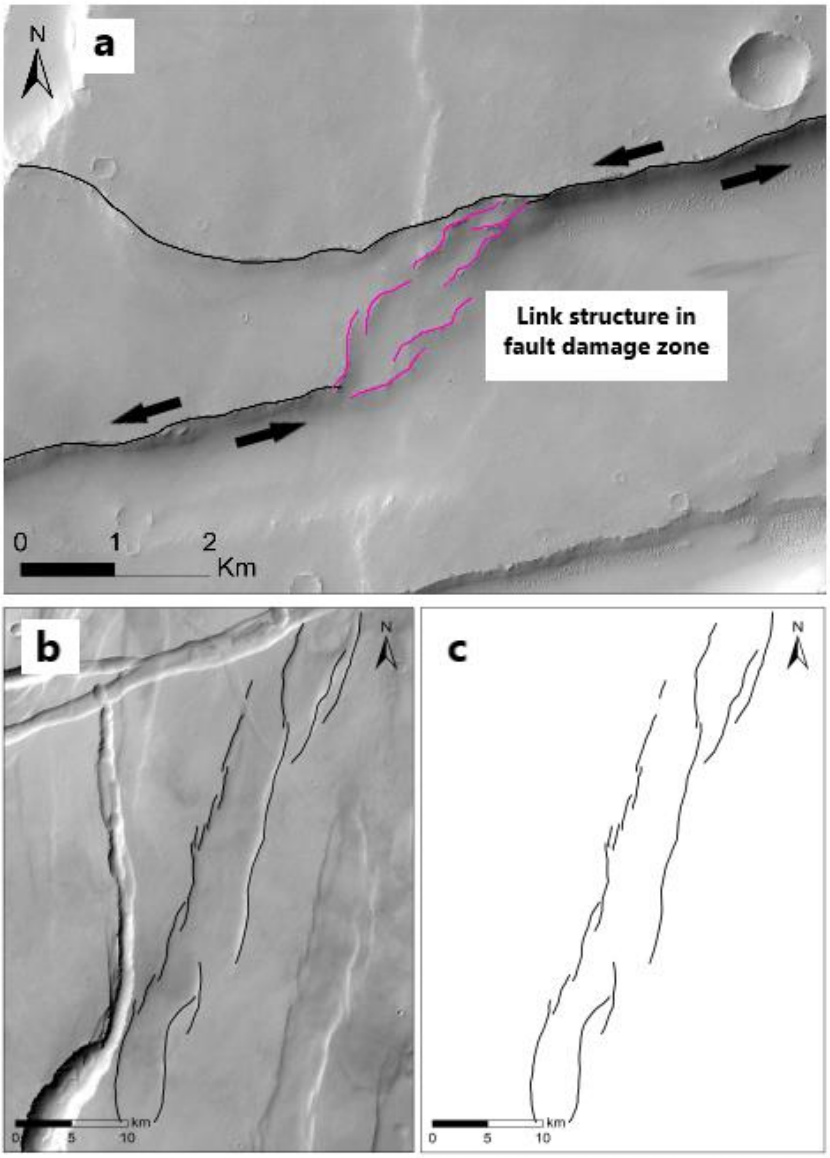

Figure 8. En-echelon of segmented faults and pull-apart structure (a) Pull-apart basin generated by sinistral transtensional kinematic of a Strike-slip fault (fault segments labelled in black lines), showing a stepover generating sidewall normal faults (Pink lines) with a left-lateral shear zone, forming an angle of 45° to the horizontal plane. View centred at 256.35°E, -5.11°N over CTX basemap (b) View over HRSC basemap, displaying a series of segments resulting from NNE-SSW principal segmented fault. (c) Interpretation background for (b), the segments are formed with the mechanism of local extension between en-echelon basement strike-slip fault segments in shear zone.

The mechanical interaction between the segments near-tip stress fields, leads to the propagation of closely spaced en-echelon toward each other [Fig.8], and the restriction of others, which consequently remain un-propagated (Walsh et al, 1999; Soliva et al., 2006; Torabi et al., 2019).

A subsidiary yet genetically related set of antithetical conjugate Riedel fractures (R') are slightly expressed among some large faults from the first system, propagating out from the main fault in an en-echelon array within active shear zones. The geometrical arrangement of these Riedel fractures is important for determining the sense of the movement within strike-slip zone and interpreting the fault kinematic.

Although faults from the three systems are repeatedly crosscutting and overlapping, we were able to classify these systems chronologically based on their superimposition. This indicates in turn that the NS and NNE-SSW faults are the older fault sets in the studied area, followed by EW and ENE-WSW faults, and lastly the NNW-SSE, NW-SE and WNW-ESE fault sets. The reactivation of some inherited faults from these systems [Fig.7], make difficulties to ensure the tectonic phase(s) related to each faut set.

3.2. Evolutionary stages of pits

Pits appear as a scalloped trough, isolated and/or connected, forming a continuous coalescent chain of diverse dimensions in Noctis Labyrinthus. These depressional surface features could extend from tens to hundreds of kilometres and are remarkably present in higher shear zones, where faults intensity and the vertical displacement of faults are significant. Surface observations show that pits lie along the graben floor, parallel or cross-cut with major and minor faults [Fig.9]. The both types of features are spatially related, coalescent, following mostly the same direction suggesting a potential mutual process for their formation. We documented a group of pit chains in strict conjunction with ENE-WSW, NNW-SSE, NNE-SSW, and EW-oriented faults, and others are closely connected to NW-SE and WNW-ESE faults [Fig.9, Fig.10].

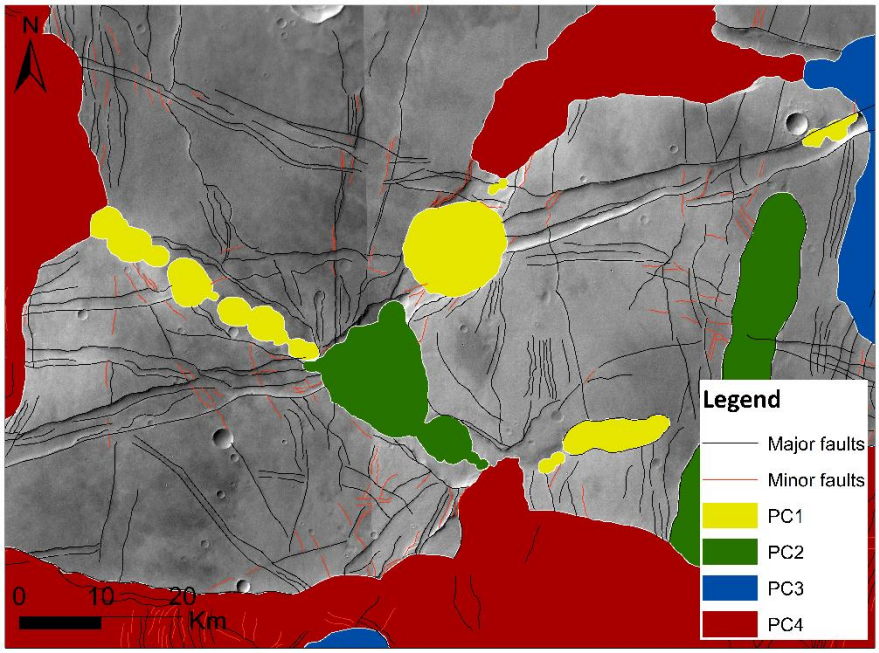

Figure 9. Regional view showing a series of pits in different evolutionary stages (PC1, PC2, PC3 and PC4), connected to swarm of major and minor faults.

This spatial relationship between faults, grabens, pits, and pit chains is supported by the azimuth dispersion in the polar plot for these surface features [Fig.10]. The polar plot for the pits and pit chains orientation shows that these depressional features are mainly oriented on NNE-SSW, ENE-WSW, and NE-SW. These trends are symmetric with the fault systems trends that have been described in Section 3.2. Although the faulting phases haven't been identified in Section 3.2, it's obvious that the pit chains are subsequent to the fault systems distribution based in the standard geological approaches used in section 3.2, to classify fault systems in relative chronological order (Childs et al., 1995). Pits and pit chains are usually overlying faults and grabens, nevertheless, few of these faults are on the top of some pits, or lying in the pit's floor, showing that these lineaments might be formed coevally with the pits and pit chains, or alternatively very close in time [Fig.9].

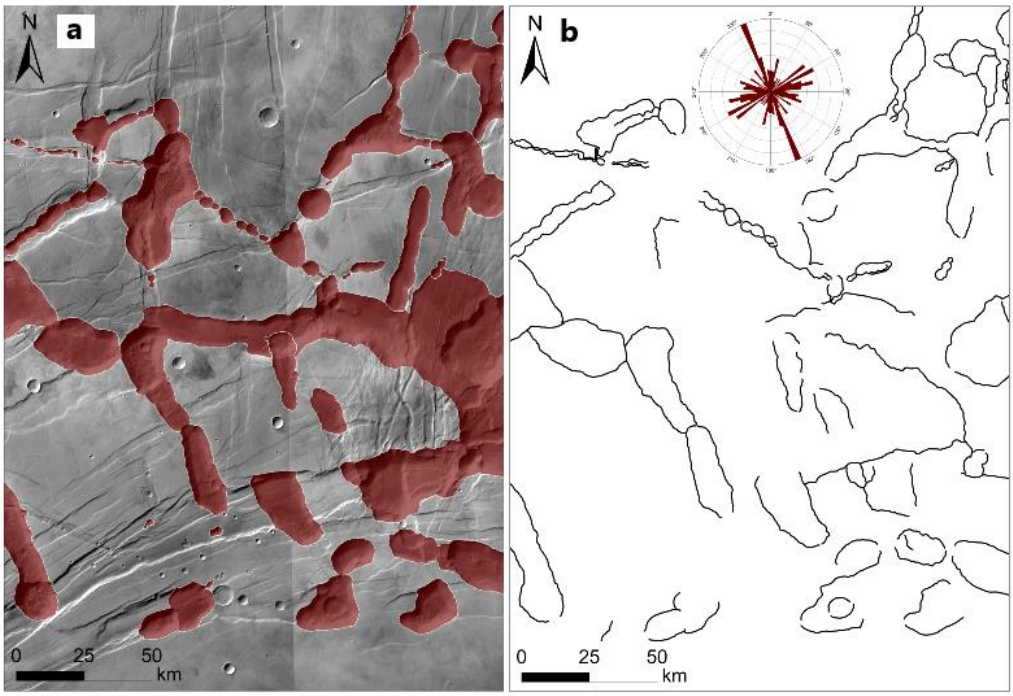

Figure 10. Pits and Pit chains mapping over HRSC basemaps. Image centered at -5,688°N_255,531°E (a) Pit chains distribution and full shape delineation (b) Pit chains boundaries interpretation background. The Pits' edge was mapped by polylines, that have been used afterward to deliver the pits orientation illustrated by the polar plot sub-figure.

In the studied area, a pre-existing graben' side which is made by two parallel faults could be erased continuously and proportionally to the mass wasting related to the surface collapse or subsidence, associated to new faults generation or pits formation. We noticed that any increase in the pits dimension (i.e., Length and width) will affect directly the apparent edge of the grabens by progressively eroding their limits. The Figure 11 show two different cases of pits-graben coalescing; by means of pits with certain dimension and spacing could be merged to form a continuous aligned chain with width strictly less than the pre-existing graben' width. In this case, the pit chains and the graben's boundaries are entirely visible [Fig.11.a]. When the graben width is relatively equal or less than the pits' width, in this case once the pits are merged to form an aligned chain. The dimension of these merged pits will increase progressively. In the most of the cases the graben's boundaries are not or maybe partially visible due to the pit chains formation that will cover and overlay the graben rim [Fig.11.b]. The Figure 11.a and 11.b show two different stages of pits, where grabens are visible although pit chains development [Fig.11.a], since pits are characterized by a relatively small dimension and they are not robustly connected. This stage defines the primitive stage for the pit chains formation. When pits are merged, and pit chains start to develop, these aligned depressional features extend over and further than the graben. As a result of this extension, the graben boundaries are not completely visible. In our observation, grabens are frequently not visible along the pit chains extension. Usually, the tail and tip of the grabens still could be identified in certain cases when pit chains overlie a graben [Fig.11.c].

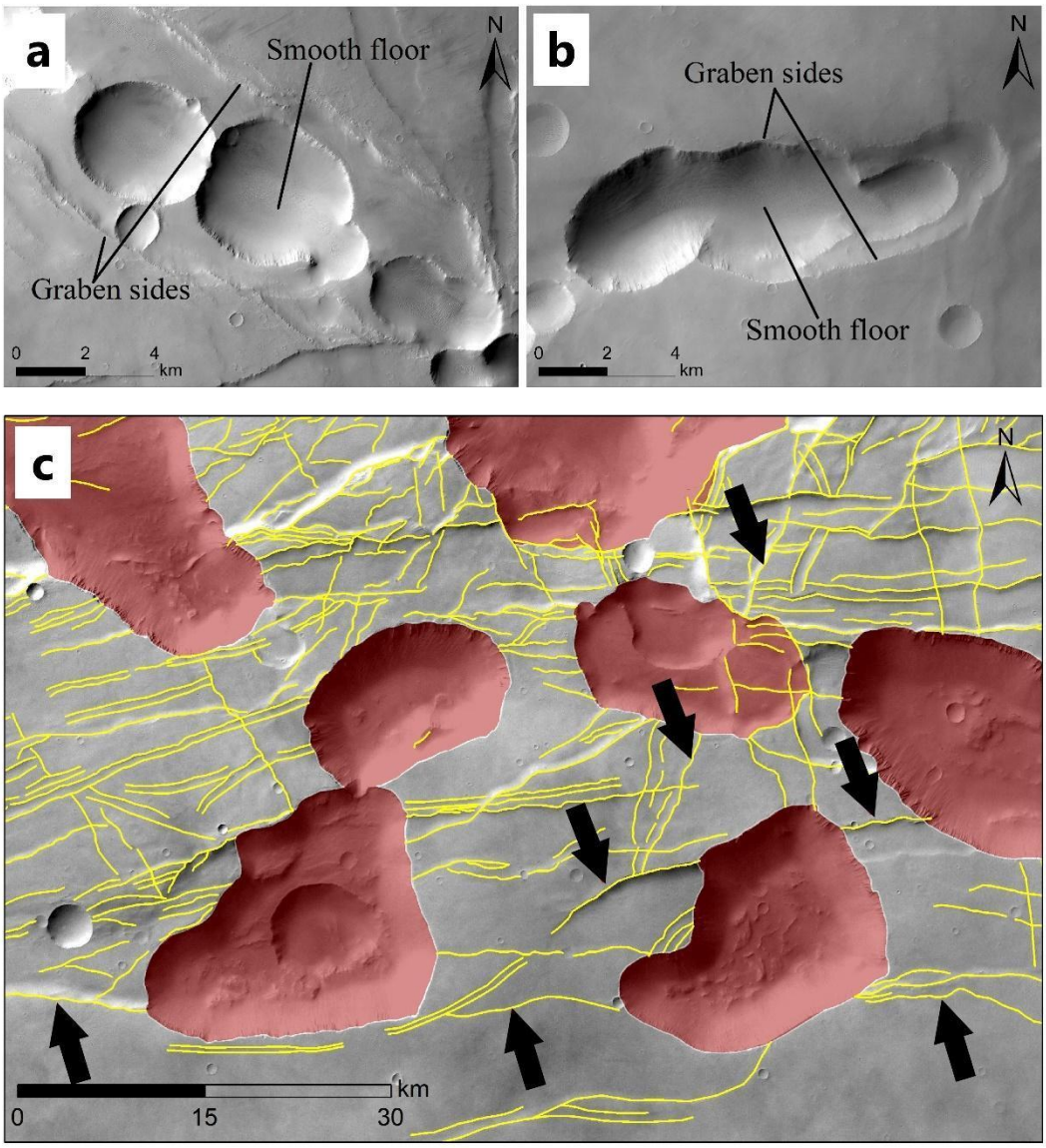

Figure 11. Cases of faults and pit chains surface interconnections. (a) Pit chains bordered by two visible parallel faults. Pits are relatively small in dimension allow the graben edges to be visible (b) Pit chains merged in advanced maturation stage compared to the pits in (a), this view shows that the pit chains obliterated the grabens rim, consequently part of the graben is no more visible. Figures (a) and (b) are made by a CTX composite imagery, showing an example of a smooth pond-like deposit on the floor of bowl-shaped pit chains (c)View of pits with different size, associated to sets of fault and graben. The arrows show the tail and tip of some faults that have been superimposed by pits. Part of these faults usually are obliterated by the pit formation or after intersection with pits.

Single and coalescing pits are characterized by different shapes and dimension that seems to be directly driven by their maturity level. Wyrick et al., 2004 explained these differences within the pits by different evolution stages. We defined the shape of pits by the following forms that have been observed in the studied area in Noctis Labyrinthus: Circular --> Elliptical -->Scalloped --> Elongated deformed. The small pits are always displayed in rounded circular shape, mostly bordered by a pair of visible parallel faults, following the pit trending. Instead, the large elongated pits show a different shape compared to the small pits, and they appear as a scalloped depressional feature in oblate form. In this case, the grabens

associated with these scalloped features are rarely observed bordering the limits because pits in this case are characterized by large width compared to adjacent grabens.

Based on the pits' morphometric attributes, we classified these surface features in four evolutionary stages as demonstrated in the figure 13. These stages are strictly controlled by the maturity level of the pits. The first stage is identified by relatively small pits, circular and holding usually a very smooth floor. In this stage, pits generally appear as a single isolated depression or sometimes slightly connected to other nearby pits, tightly bordered by two or more visible parallel faults, expressed along the graben's floor, and rarely interacting with the graben edge. The second stage show pits closely connected to each other, creating an aligned chain that extends for tens of kilometres. Pits in this level start losing their rounded shape and become deformed, they display as an oblate trough. The third stage is identified by a deformed lobate shape of pits due to mass wasting and landslides at the pits' borders. Pits in this stage became very deformed and robustly connected to extensional faults and/or graben around, often overlapping faults. In this situation, the graben's width is inferior to that of the pits and pit chains. Thus, major group of the graben is erased by the pit chains' formation and size increase. The last evolutionary stage for the pits is the most critical one. In this level, pits are characterized by a significant deformed shape and large size. Some pits are filled by hummocky deposits, indicating wasting processes derived by the collapse of their bounding walls on which ample arched-shaped niches are sometimes visible.

Some pits present wrinkle ridges along their floor [Fig.12]. These features are quasi-linear to arcuate asymmetric topographic highs, identified as complex compression structures observed usually on the volcanic surfaces. Wrinkle ridges form when tectonic forces compress an elastic lava sheet. In the studied area of Noctis Labyrinthus, the wrinkle ridges have been essentially identified on the floor the pits and pit chains, and intercrater plains. Other pits have smooth, flat floors, potentially related to lava flow erosion during the pits' formation. Similar depressional features have been studied in Ascraeus Mons and thought to involve a volcanic process (Pozzobon et al., 2014). The conjunction pit-graben shows a higher vertical displacement reaching up to 3.6 km with respect to single isolated graben.

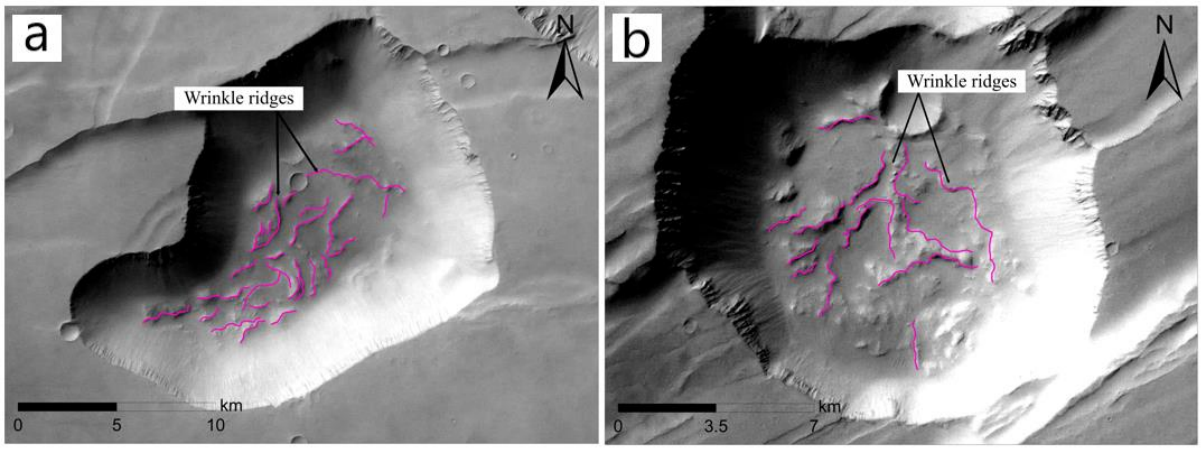

Figure 12. View of pits with some wrinkle ridges in their floor. (a) Single isolated pit crosscutting with fault, displaying a smooth floor with clustering small wrinkle ridges. (b) Scalloped pit connected to adjacent pits. The floor of the pit shows short sinuous arch of wrinkle ridges of asymmetric topographic high.

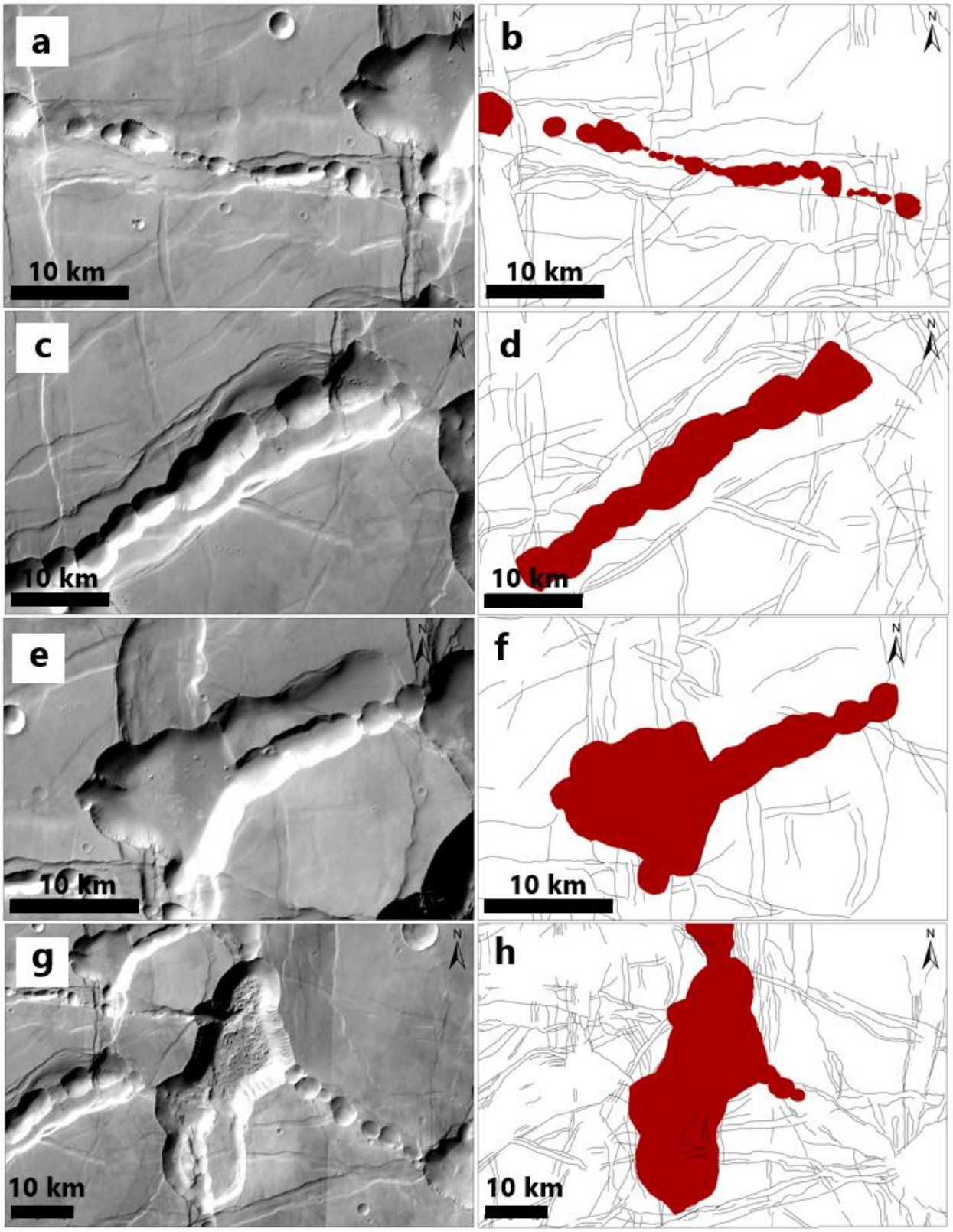

Figure 13. Sketch for the different evolutionary stages of the pit chains formation in Noctis Labyrinthus. The figures (a), (c), (e) and (g) are respectively the 1st, 2nd, 3rd and 4th stage for the pit chains formation. The (b), (d), (f) and (h) figures are respectively the background interpretation for the stages (a), (c), (e) and (g).

4.Discussion

The investigation of the structural map [Fig. 5] helped to study the global spatial distribution and trending of faults. This study has a direct impact on understanding the faults kinematic and the tectonic setting of the region. The faults that have been mapped in this work are normal faults, with minor contributions of some left and right strike-slip faults. Indeed, the fault systems identified based on the faults trending, crosscutting relationship and superimposition are generated by more than one tectonic and magmatic events. These systems display different orientations and spatial distributions, suggesting different processes and shear stresses origin for their formation.

The first system made by NS and NNE-SSW oriented faults [Fig.6] implies an extension in the EW and ESE-WNW, respectively. This extension is expressed by a pull-apart basin [Fig.8.a] generated by sinistral transtensional kinematic of a strike-slip fault, alongside the stepovers and en-echelon faults [Fig.8.b and 8.c] within NNE- SSW and NS faults. The right and left-lateral transtentional kinematics among the first system results in strain ellipsoids, implies a state of homogenous strain that tend to be a flattening (i.e., Pancake shape $X \geq Y >> Z$). This strain explains the rectangular extensional blocks obviously present on the northmost [Fig.7.a]. We suggest that NS and NNE-SSW fault system accommodates a coeval lateral extension from a driving stress tensor, probably associated with the formation of Valles Marineris. We link this system to two successive tectonic phases. Each phase consists of a bidirectional deformation. The first bidirectional phase produced the NS faults and the western EW slight bending of the Valles Marineris by two phases of $\perp$ uniaxial extension on the EW and NS, respectively. The second bidirectional phase produced NNE-SSW faults together with the ESE-WNW bending for the Valles Marineris by two phases of $\perp$ uniaxial extension, respectively in ESE-WNW and NNE-SSW. The reorientation of the Valles Marineris bending from the ESE-WNW to EW invokes the reorientation of the stress field from NNE to NS, which explains the presence of the strike-slip faults among the first system. The relative age for the first fault system was not determined in this study, but it is thought to belong to the age of Valles Marineris' formation (i.e., Late-Hesperian). We interpreted this system to be purely tectonic in origin.

The second system is formed by ENE-WSW and EW fault sets, not coeval with the faults from the previous system, and seem to be generated by a diverse process and has a diverse origin. This observation is supported by the spatial distribution and the fault orientations of this system compared to the first one [Fig.6]. Intensive groups of ENE-WSW and EW faults are remarkably observed in the south, closer and connected to pits and pit chains. Many of these faults appear concentric to Syria Planum, developing from the south as ENE-WSW lineaments and deviate afterward to be EW trending faults, appearing arcuate and creating an angle of ~90 to the north. We interpreted these swarms of ENE-WSW and EW concentric and parallel faults to be generated by a radial oblate stress tensor, likely related to Syria Planum volcanic province. This interpretation was based on the volcano-tectonic background of Syria Planum and Noctis Fossae (Pieterek et al., 2022, Baptista et al., 2008; Pozzobon et al., 2023). The radially prominent grabens' swarms around Syria Planum led to propose that this province underwent an extensional tectonic, which was probably initiated in the Late Noachian according to Tanaka & Davis., 1988, and seems to be driving the formation of the arcuate concentric ENE-WSW and EW faults in Noctis Labyrinthus through a flexural uplift, accompanied by the formation the Syria Planum small shield volcanoes. Alternatively, these arcuate concentric faults and grabens might be generated by Noctis Labyrinthus' NS faults formation within an oblate strain or the Valles Marineris' ESE-WNW to EW bending that might also play a role in the formation of these arcuate faults. However, the NS faults that we identified in the first system could also be coeval of the slight EW faults from the second fault system. Thus, this might provide the context of synchronous bi-directional extension of faults from the first and the second systems. The analysis of the second system shows that faults cannot be driven by the extensional tectonic as the only process for their formation. Still, apparently the magmatic plumbing

related to the Syria Planum volcanic province has been engaged. This magmatic plumbing in Syria planum seems to be behind the generation of the arctic fault system displayed by the ENE-WSW deviating to EW toward the EW bending of Valles Mariners. We interpreted these faults as an inclined sheet for a magma chamber underneath Syria Planum volcanic province, generated in the context of synchronous bidirectional extension: Two uniaxial extensions on the NS and NNW-SSE through individual tectonic phase, responsible for the formation of the ENE-WSW and EW faults. We believe that the second fault system is formed in response to the magma transport from deep to the surface through dikes (Fialko et al., 1999; Gudmundsson., 1990,2000,2006; Mège, &Korme., 2004; Chen & Jin., 2006). This transport generates a stress in the rock mass that will lead to surface collapse, responsible about ENE-WSW and EW fault and graben sets. We interpreted this system to be generated by surface collapse of magmatic origin.

The third system contains faults trending in the NNW-SSE, NW-SE, and NW-SE, characterized by a minor azimuth distribution and displayed very close to pits and pit chains. These faults are slightly disseminated in the north and are more intense in pits area. Sometimes, they appear along the pit chains floor, intersecting with the edge of pits, indicating a relatively younger age with respect to previous fault systems. Faults and grabens from this system seem to be aliens compared to the pre-existing faults from ENE-WSW, EW, NE, and NNE-SSW. The third system appears to be related to external driving processes outside the Noctis Labyrinthus province, and likely might be related to Tharsis province. This observation is supported by the well-known significant tectonic activity of Tharsis region (Wise et al., 1979; Plescia & Saunders., 1982; Tanaka et al., 1991; Plescia., 1991; Mège & Masson., 1996; Okubo et al., 2006). The tectonic phase(s) responsible for this system is still in discussion for further future work. We interpreted this system to be related to the ending appendage for a volcanic and extensional movement in the northwest of Noctis Labyrinthus, potentially within the Tharsis rise.

Based on our studies for the different fault systems, we agree with some systems that have been cited by Masson., 1977. However, we argue that the trends of each system that have a direct impact for the chronology of the faulting phases, the sequence of the events, and the tectonic history led to the formation of Noctis Labyrinthus. The important volcanic behaviour of Syria Planum (Baptista et al., 2008; Pozzobon et al., 2023) was not properly engaged in the previous model proposed for Noctis Labyrinthus (Wyrick et al., 2004, Rodriguez et al., 2016, Chavan et al., 2022). This implies a deficient interpretations and incomplete model for the formation of Noctis Labyrinthus, that does not consider the Volcano-Tectonic background of the adjacent centers in the region.

The extensive analysis of the faults' distribution by Tanaka & Davis., 1988 for the Tharsis region led to identify six distinct episodes of tectonic events, mainly Syria Planum – Centred activity. We therefore believe that the studies of Tanaka & Davis., 1988 might be overestimating the role of Syria Planum's tectonic activity within the Tharsis region due to the inability to resolve and characterize the faults properties in lower resolution datasets, or the overmapping of fault and graben sets. In addition, the progression of the faulting episodes suggested by Chavan et al., 2022, the fault sets, and the diving events likely need revision and further detailed studies. Previous studies also potentially require a review for the fault systems, tectonic phases and the related events (Masson., 1977; Tanaka & Davis., 1988; Mège & Masson.,1996; Schultz., 1998; Mège et al., 2003; Bistacchi et al., 2004; Montgomery et al., 2009; Kling et al., 2021;Chavan et al., 2022).

The strong correlation between faults, grabens, and pit chains is indeed related to common processes for their formation. The previous studies citing the dilational faulting on groundwater flow be evaluated fully without any magmatic origin (Wyrick et al., 2004; Weitz et al., 2011, 2013, 2014; Rodriguez et al., 2016; Baioni et al.,2017; Baioni., 2018) or a tectonic and volatile-related processes (Kling et al., 2021), might require further work, give thought to the tectonic and volcanic background of the region.

The spatial surface interconnection between Faults-Grabens-Pits could be genetically related to the mechanism behind their formation. This interpretation is propped by the pits and pit chains orientation in the polar plot [Fig.10] which demonstrates that pits are always trending in the same directions as the fault systems on NNE-SSW, ENE-WSW, and NE-SW. This observation has a direct impact on suggesting a common process behind the formation of pit chains and NNE-SSW, ENE-WSW, and NE-SW trending faults. The formation of pits seems to be occurring in higher strain zones, where the faults intensity distribution is significant compared to other areas.

The mapping of the pits and pit chains [Fig. 5] helped not only to study their distribution and relationship to the faults, but also it identified different evolutionary stages for these depressional features. The evolutionary stages of the pit chains documented in Wyrick et al., 2004 in the eastern Alba Patera, have been integrated in this work. However, we are proposing different stages, based on the pits shape, size, and degree of connection to adjacent pits. We classified the trough identified by Wyrick et al., 2004 as the final stage of the pits' formation in Noctis Labyrinthus.

These stages [Fig.5] are directly associated with the pits' maturity level that cannot be controlled only by the extensional tectonic. The pits and pit chains show a curative limit and a rounded scalloped shape, which indeed cannot be tectonic in origin. Thus, the magmatic origin for these features is highly acknowledged in this work, and this could be supported by the presence of wrinkle ridges in the pits floor [Fig.12]. The deformed shapes of the pits and the proportional relationship for their geometrical attributes (i.e., Length, width, vertical displacement, and shape) led to deem them as a feature of Volcano-Tectonic origin, rather than tectonic. Moreover, the important enlargement of the pits' morphometrics attributes (i.e., Length, width and shape) compared to purely tectonic features such grabens and faults, is likely caused by the surface collapse related to magma plumbing in the subsurface or a lava flow, which is at the base of the erosional evolution catena (Pit chains) → Fossa →Valles →Chasma, as observed in the Coprates region of Mars (Leone., 2014).

The vertical displacement of the graben is directly controlled by the graben formation, thus the intensity of the crustal extension. Instead, the pits and pit chains' vertical displacement seem to be affected by a first surface collapse related to the pre-existing faults or grabens, and a second collapse related to the pits' formation. Once the pit chains start forming along the graben floor, an additional stress field will be added to the existing graben due to the magma-plumbing system underneath the graben.

The formation of the pits and pit chains start when the floor of the pre-existing grabens and faults fall down once the magma chamber initiates its deflation after the complete formation and reactivation of the first and second systems of fault. The third system of faults seems to be simultaneous or proximate to the pit chains formation. The formation of pits and the development of their size and shape progressively erode the pre-existing graben rims, which explains the partial presence of the graben's boundaries in some cases [Fig.11.b]. The vertical displacement between the Pit-Graben joint feature does not represent the real vertical displacement of the graben, nor of the pits, but rather the product of the vertical displacement for both features after two episodes of surface collapse related to the pits' formation along the graben and to the pre-existing graben' formation driven by the crustal extension. Several pits studied in this work display a very smooth floor, indicating a potentially resurfacing that might be related to a volcanic flow. Although pits and pit chain formation is still a subject for further detailed studies, we suggest that these features are produced by pressure drops related to the collapse of magma chamber underneath the graben.

Previous studies from Chavan et al., 2022; Kakaria & Yin., 2023 speculated fluvial and subglacial activity for the trough networks in Noctis Labyrinthus. We acknowledged the possibility of collapse-driven by the Caldera subsidence for the formation of the pit chains in Noctis Labyrinthus, based in analogue modelling and laboratory experiments by Lavallée et al., 2004; Acocella., 2007; Cushing et al., 2015. Unlike Wyrick et al., 2004, the magma pathway that requires the presence of the dikes and a magma

chamber deflation is needed for the model we are proposing to form pits and pit chains in Noctis Labyrinthus.

5. Conclusion

In this work, we conclude that the formational history of Noctis Labyrinthus is represented by a complex sequence of events that led to complex surface features characterising this region of Mars. The fault systems in Noctis Labyrinthus are produced by not regionally-Centred extensive tectonic, displayed by dip-slip and strike-slip faults.

We explain the formational history of Noctis Labyinthus as follows:

- The first fault system in the studied area is produced by two major phases of bidirectional deformation: The first bidirectional tectonic phase produced the NS faults and the western EW slight bending of the Valles Marineris, within two phases of ⊥ uniaxial extension on the EW and NS. The second bidirectional phase predominantly accommodates crustal extension associated with transtensional movement. During this phase, a set of NNE-SSW faults was generated with the ESE-WNW bending for the Valles Marineris, by two phases of ⊥ uniaxial extension on the ESE-WNW and NNE-SSW. We believe that the production of the first fault system is purely tectonic in origin [Fig.14.a]. During the formation of this system the magma source at depth starts preparation to rise for upper level, without any involvement in the formation of the first fault system.
- The second fault system represented by the ENE-WSW and EW-oriented faults and grabens is developed through radial oblate stress. This tensor associated with first surface collapse of magmatic origin related to magma transport from the magma chamber to the surface through dikes. Dikes in this level are potentially the feeder system to the magma flow that comes from magmatic source [Fig.14.b]. The transport of magma from the magmatic chamber to the surface is substantially important in term of time. We associated the magmatic plumbing responsible about the formation of this system to Syria Planum volcanic province. The small shield volcanoes of Syria Planum and the magmatic flow probably extending under Noctis Labyrinthus bulk. This will produce a stress field that generate the formation of concentric grabens around the magma source represented by an inclined sheet, explaining the ENE-WSW faults that change afterward to EW trending faults.
- After the complete set and the reactivation of some inherited faults from the first and second fault systems [Fig.14.c], the third system of NNW-SSE, NW-SE, and NW-SE faults start to form before, or simultaneously appears within the pits and pits chains formation [Fig.14.d]. This fault system has not been associated with any specific tectonic phases in this work. Its origin is still in debate for further future work, CTX dataset will enhance more insight, however the Tharsis province's tectonic and volcanic activity is acknowledged. The exact temporal relation between the third fault system and the pit chains is still in discussion, but we believe that their formation is proximate or simultaneous.
- Once the magma rises and lava flow transport to the surface is completed alongside the second fault system formation, the magma chamber deflates progressively after a crust uplift, which will cause a second surface collapse of magmatic origin related to the magma chamber deflation. At this stage, pits and pit chain start forming in weak and fault damage zones, where faults and grabens are displayed with high intensity of distribution [Fig.14.d]. The formation of these depressional surface features in Noctis Labyrinthus show an important interconnection between the fault systems, pits and pit chains formation. This in turn display an important interaction between crustal faulting and crustal magmatic circulation and accumulation.

The proposed model ties together an early extensional tectonic and magmatic plumbing [Fig.14], as a reasonable assumption to explain the formational history of Noctis Labyrinthus.

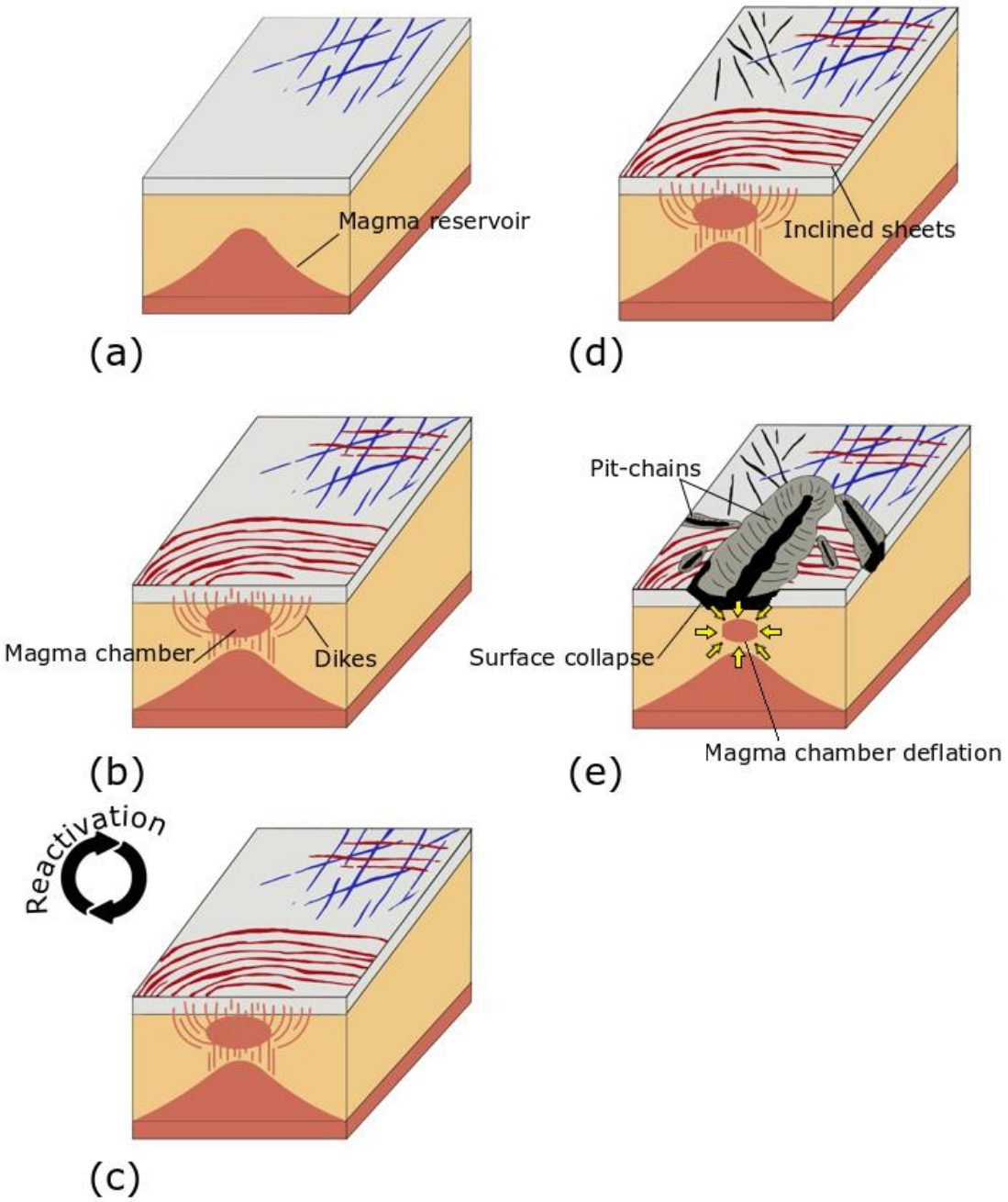

Figure 14. Sketch showing the sequence of events responsible about the formation of Noctis Labyrinthus (a) First fault system produced by two phases of bi-directional extension, represented by NS and NNE-SSW trending faults (b) Second system of fault represented by ENE-WSW and EW trending faults. These faults have been interpreted as inclined sheets, related to the magmatic activity in Syria Planum (c) The reactivation phase of some inherited faults from the first and second systems (d) Third fault system formation, represented by NNW-SSE, NW-SE and WNW-ESE oriented faults. The temporal formation of this system relatively to the pits still uncertain. The origin of these faults seems to be related to the Tharsis province (e) Pits and pit chains formation along grabens floor, after magma chamber deflation and surface collapse.

Acknowledgments

The authors would like to thank the reviewers for all their thoughtful comments and efforts towards improving our manuscript. This work was supported by the ESA Archival Research Visitor Programme using the HRSC archive, and the Centre for Studies and Activities for Space - CISAS, University of Padova. We acknowledge support from ESA through the Science Faculty - Funding reference ESA-SCI-SC-LE-209.

Declaration of Competing Interest

The authors declare that they have no known competing financial interests or personal relationships that could have appeared to influence the work reported.

References

Cushing, E.G., Okubo,H.C., Titus, N.T., 2015. Atypical pit craters on Mars: New insights from THEMIS, CTX, and HiRISE observations. J. Geophys. Res. 120 (6), 1023-1043. doi: https://doi.org/10.1002/2014JE004735

El Yazidi, M., 2023. Structural analysis of the fault networks in Noctis Labyrinthus (Mars) and preliminary geological mapping for 1/2 of the Eminescu (H09) quadrangle in Mercury. IRIS, Catalogo Ricerca UNIPD, 08.01 - Tesi di Dottorato UNIPD. https://hdl.handle.net/11577/3469755

Sauro, F., Pozzobon, R., Massironi, M., De Berardinis, P., Santagata, T., De Waele, J., 2020. Lava tubes on Earth, Moon and Mars: a review on their size and morphology revealed by comparative planetology. Earth. Sci. Rev. 209, 103288. doi: https://doi.org/10.1016/j.earscirev.2020.103288

Luzzi, E., Pio Rossi, A., Carli, C., Altieri, F., 2020.Tectono-Magmatic, Sedimentary, and Hydrothermal History of Arsinoes and Pyrrhae Chaos, Mars. J. Geophys. Res. 125 (12), e2019JE006341. doi: https://doi.org/10.1029/2019JE006341

Kling, C. L., Byrne, P. K., Atkins, R. M., Wegmann, K. W., 2021. Tectonic deformation and volatile loss in the formation of Noctis Labyrinthus, Mars. J. Geophys. Res. Planets.126 (11), e2020JE006555. doi: https://doi.org/10.1029/2020JE006555

Pozzobon, R., Orlandi, D., Pagli, C., Mazzarini, F., 2021. Volcano dynamics vs. tectonics on Mars: Evidence from Pavonis Mons; J. Volcanol. Geotherm. Res. 410, 107148. doi: https://doi.org/10.1016/j.jvolgeores.2020.107148

Lucchitta, B.K., McEwen, A.S., Clow, G.D., Geissler, P.E.,Singer, R.B., Schultz, R.A., and Squyres, S.W., 1992. The canyon system of Mars. In Kieffer, H.H., et al (Eds). Mars. Univ. of Ariz. Press, 453-492.

Lucchitta, B.K., Isbell, N.K., Howington. -Kraus. A., 1994. Topography of Valles Marineris: implications for erosional and structural history. J. Geophys. Res.99 (E2), 3783-3798. doi: https://doi.org/10.1029/93JE03095

Carr, M.H., 1974.Tectonism and volcanism of the Tharsis region of Mars. J. Geophys. Res. 79 (26), 3943-3949. doi: https://doi.org/10.1029/JB079i026p03943

Masson, P.,1985. Origin and evolution of Valles Marineris region of Mars. Adv.Space.Res. 5 (8), 83-92. doi:https://doi.org/10.1016/0273-1177(85)90244-3

Schultz, R.A.,1995. Gradients in extension and strain at Valles Marineris, Mars. Planet. Space Sci. 43 (12), 1561-1566. doi: https://doi.org/10.1016/0032-0633(95)00111-5

Mège, D., Bourgeois, O., 2011. Equatorial glaciations on Mars revealed by gravitational collapse of Valles Marineriswallslopes. Earth Planet. Sci. Lett. 310 (3-4), 182-191. doi: https://doi.org/10.1016/j.epsl.2011.08.030

Andrews-Hanna, J.C., Zuber, M. T& Hauck, S.A., 2008a.Strike-slip faults on Mars: Observations and implications for global tectonics and geodynamics. J. Geophys. Res. Planets. 113 (E8). doi: https://doi.org/doi:10.1029/2007JE002980

Andrews-Hanna, J.C., 2012b. The formation of Valles Marineris:1. Tectonic architecture and the relative roles of extension and subsidence. J. Geophys. Res. Planets.117 (E3). doi: https://doi.org/10.1029/2011JE003953

Brustel.C.,Flahaut, J., Hauber, E., Fueten, F., Quantin, C., Stesky, R., Davies, G.R., 2017. Valles Marineris tectonic and volcanic history inferred from dikes in eastern Coprates Chasma. J. Geophys. Res. Planets, 122 (6), 1353-1371. doi: https://doi.org/10.1002/2016JE005231

Anderson, R.C., Dohm, J.M., Golombek, M.P., Albert, F.C., Franklin,B.J., Tanaka, K.L., Lias, J., Peer, B., 2001. Primary centers and secondary concentrations of tectonic activity through time in the western hemisphere of Mars. J. Geophys. Res., 106 (E9), 20563-20585. https://doi.org/10.1029/2000JE001278

Richardson, J.A., Bleacher, J.E., Glaze, L.S., 2013. The volcanic history of Syria Planum, Mars. J. Volcanol. Geotherm. Res. 252, 1-13. doi: http://dx.doi.org/10.1016/j.jvolgeores.2012.11.007

Greeley, R & Spudis, P.D., 1981.Volcanism on mars. Rev. Geophys. 19 (1),13-41. doi: https://doi.org/10.1029/RG019i001p00013

Head, J. W., Kreslavsky, M. A., S. Pratt., 2002. Northern lowlands of Mars: Evidence for widespread volcanic flooding and tectonic deformation in the Hesperian Period. J. Geophys. Res. Planet.107 (E1), 3-29. doi: http://dx.doi.org/10.1029/2000JE001445

Johnson, C.L., Phillips, R.J., 2005. Evolution of the Tharsis region of Mars: insights from magnetic field observations. Earth Planet. Sci. Lett.230 (3-4), 241-254. doi: https://doi.org/doi:10.1016/j.epsl.2004.10.038

Baker, V., Maruyama, S., Dohm, J., 2007. Tharsis Superplume and the Geological Evolution of Early Mars. In: Yuen, D.A., Maruyama, S., Karato, SI., Windley, B.F. (eds) Superplumes: Beyond Plate Tectonics. Springer, Dordrecht. doi: https://doi.org/10.1007/978-1-4020-5750-2_16

Dohm, J.M., Baker, V.R., Maruyama, S., Anderson, R.C., 2007. Traits and evolution of the Tharsis superplume, Mars. In: Yuen, D.A., Maruyama, S., Karato, S.-I., Windley, B.F. (Eds.), Superplumes: Beyond Plate Tectonics. Springer, 523-537. doi: http://dx.doi.org/10.1007/978-1-4020-5750-2_17

Hauber, E., Brož, P., Jagert, F., Jodłowski, P., Platz, T., 2011. Very recent and wide-spread basaltic volcanism on Mars. Geophys. Res. Lett. 38 (10), 1-5.doi: https://doi.org/doi:10.1029/2011GL047310

Beuthe, M., Le Maistre, S., Rosenblatt, P., Pätzold, M., Dehant, V., 2012. Density and lithospheric thickness of the Tharsis Province from MEX MaRS and MRO gravity data. J. Geophys. Res. Planets, 117 (E4). doi: https://doi.org/10.1029/2011JE003976

Leone, G., 2021. The Formation of Mars and the Origin of Its Volcanic Provinces, in: Mars: A Volcanic World. Springer, Cham, Cham. 19–50. doi: https://doi.org/10.1007/978-3-030-84103-4_2

Leone, G., Grosse, P., Ahrens, C., Gasparri, D., 2022. Geomorphological and morphometric characteristics of the volcanic edifices along a volcanic alignment of Tharsis on Mars. Geomorphology. 414, 108385.doi: https://doi.org/10.1016/J.GEOMORPH.2022.108385

Bouley, S., Baratoux, D., Paulien, N., Missenard, Y., Saint-Bézar, B., 2018. The revised tectonic history of Tharsis. Earth Planet. Sci. Lett. 488,126-133. https://doi.org/10.1016/j.epsl.2018.02.019

Anderson, R.C., Dohm, J.M., Haldemann, A.F.C., Hare, T.M & Baker, V.R., 2004. Tectonic histories between Alba Patera and Syria Planum, Mars. Icarus. 171 (1), 31-38. doi: http://dx.doi.org/10.1016/j.icarus.2004.04.018

Yin, A., 2012. An episodic slab-rollback model for the origin of the Tharsis rise on Mars: Implications for initiation of local plate subduction and final unification of a kinematically linked global plate-tectonic network on Earth. Lithosphere. 4 (6), 553-593. doi: https://doi.org/10.1130/L195.1

Tanaka, K.L., Davis, P.A., 1988. Tectonic history of the Syria planum province of Mars. J. Geophys. Res. Solid Earth. 93 (B12), 14893-14917. doi: https://doi.org/10.1029/JB093iB12p14893

Mège, D., Masson, P., 1996. A plume tectonics model for the Tharsis province, Mars. Planet. Space Sci. 44 (12),1499-1546. doi: https://doi.org/10.1016/S0032-0633(96)00113-4

Rodriguez, J.A.P., Zarroca, M., Linares, R., Gulick, V., Weitz, C.M., Yan, J., Fairén, A.G., Miyamoto, H., Platz, T., Baker, V., Kargel, J., Glines, N., Higuchi, K., 2016. Groundwater flow induced collapse and foolding in Noctis Labyrinthus, Mars. Planet. Space Sci.124, 1-14. doi: https://doi.org/10.1016/j.pss.2015.12.009

Baioni, D., 2018. Karst Landforms as markers of recent climate change on Mars: An example from a late amazonian epoch evaporate-karst within a trough in western Noctis Labyrinthus. Recent and Current Landscape Evolution of the Red Planet. In: Dynamic Mars. Elsevier, 411-429. doi: https://doi.org/10.1016/B978-0-12-813018-6.00014-5

Weitz, C.M., Bishop, J.L., Grant, J.A., 2013. Gypsum, opal, and fluvial channels within a trough of Noctis Labyrinthus, Mars: implications for aqueous activity during the late Hesperian to Amazonian. Planet. Space Sci.87, 130-145. doi: https://doi.org/10.1016/j.pss.2013.08.007

Weitz, C.M & Bishop, J.L., 2014. Diversity of hydrated minerals and deposits at Noctis Labyrinthus: implications for the late Hesperian to Amazonian aqueous activity on Mars. Int. Conf. Mars. 1791, 1222. Bibcode: 2014LPICo1791.1222W

Wyrick, D., Ferrill, D.A., Morris, A.P., Colton, S.L., Sims, D.W., 2004. Distribution, morphology, and origins of Martian pit crater chains. J. Geophys. Res.109(E6), E06005. doi: http://dx.doi.org/10.1029/2004JE002240

Leone, G., 2014. A network of lava tubes as the origin of Labyrinthus Noctis and Valles Marineris on Mars. J. Volcanol. Geotherm. 277, 1-8. doi: http://dx.doi.org/10.1016/j.jvolgeores.2014.01.011

Schultz, R.A., 1998. Multiple-process origin of Valles Marineris basins and troughs, Mars. Planet. Space.Sci. 46 (6-7), 827-834. doi: https://doi.org/10.1016/S0032-0633(98)00030-0

Dohm, J.M., Williams, J.-P., Anderson, R.C., Ruiz, J., McGuire, P.C., Komatsu, G., Davila, A.F., Ferris, J.C., Schulze-Makuch, D., Baker, V.R., Boynton, W.V., Fairen, A.G., Hare, T.M., Miyamoto, H., Tanaka, K.L., Wheelock, S.J., 2009. New evidence for a magmatic influence on the origin of Valles Marineries, Mars. J. Volcanol. Geotherm. Res.185 (1-2), 12-27. doi: http://dx.doi.org/10.1016/j.jvolgeores.2008.11.029

Masson, P., 1977. Structure Pattern analysis of Noctis Labyrinthus-Valles Marineris regions of Mars. Icarus. 30 (1), 49-62. doi: http://dx.doi.org/10.1016/0019-1035(77)90120-8

Kakaria,R., Yin, A., 2023. Subglacial catastrophic-flood origin of linear and curvilinear flat-rimmed pit chains on Mars: Evidence from geomorphological mapping and detailed landsystem analysis. Icarus. 395,115439. doi: https://doi.org/10.1016/j.icarus.2023.115439

Pozzobon, R., Mazzarini, M.,Isola, I., 2023. Deep and shallow crustal structure control on the late-stage volcanism in Syria Planum (Mars). J. Volcanol. Geotherm. Res. 439, 107830. doi: https://doi.org/10.1016/j.jvolgeores.2023.107830

Pieterek,B., Laban, M., Ciążela, J., Muszyński, A., 2022. Explosive volcanism in Noctis Fossae on Mars. Icarus. 375,114851. doi: https://doi.org/10.1016/j.icarus.2021.114851

Lavallée, Y., Stix, J., Kennedy, B., Richer, M., Longpré, M.A., 2004. Caldera subsidence in areas of variable topographic relief: results from analogue modeling. J. Volcanol. Geotherm. Res. 129 (1-3), 219-236. doi: https://doi.org/10.1016/S0377-0273(03)00241-5

Acocella, V., 2007. Understanding caldera structure and development: An overview of analogue models compared to natural calderas. Earth Sci Rev. 85 (3-4), 125-160. doi: https://doi.org/10.1016/j.earscirev.2007.08.004

Baioni, D., Tramontana, M & Hajna, N. Z., 2017. Karst landforms Within Noctis Labyrinthus, Mars. Acta Carsologica. 46 (1), 73-82. doi:https://doi.org/10.3986/ac.v46i1.4704

Weitz, C.M., Bishop, J.L., Thollot, P., Mangold, N., Roach, L.H., 2011. Diverse mineralogies in two troughs of Noctis Labyrinthus, Mars. Geology. 39 (10), 899-902. doi: http://dx.doi.org/10.1130/G32045.1

Mège, D., Cook, A. C., Garel, E., Lagabrielle, Y., Cormier, M.H., 2003. Volcanic rifting at Martian grabens. J. Geophys. Res.108 (E5), E55044. doi:https://doi.org/10.1029/2002JE001852

Bistacchi, N., Massironi, M., Baggio, P., 2004. Large-scale fault kinematic analysis in Noctis Labyrinthus (Mars). Planet. Space Sci.52 (1-3), 215-222. doi: https://doi.org/10.1016/j.pss.2003.08.015

Baptista, A. R., Mangold, N., Ansan,V., Baratoux, D., Lognonné, P., Alves, E. I., Williams, D. A., Bleacher, J. E., Masson, P., &Neukum, G., 2008. A swarm of small shield volcanoes on Syria Planum, Mars. J. Geophys. Res.113 (E9). doi: https://doi.org/10.1029/2007JE002945

Childs, C., Watterson, J., Walsh, J.J., 1995. Fault overlap zones within developing normal fault systems. Geol. Soc. Spec. Publ.152 (3), 535-549. doi: https://doi.org/10.1144/gsjgs.152.3.0535

Aydin, A & Schultz, R.A., 1990. Effect of mechanical interaction on the development of strike-slip faults with echelon patterns. J. Struct. Geol.12 (1), 123-129. doi: https://doi.org/10.1016/0191-8141(90)90053-2

Peacock, D. C. P., Sanderson, D. J., 1991. Displacement, segment linkage and relay ramps in normal fault zones. J. Struct. Geol.13 (6), 721-733. doi: https://doi.org/10.1016/0191-8141(91)90033-F

Brent, M.R & Cartwright, T.A., 1996. Distributional regularity and phonotactic constraints are useful for segmentation. Cognition. 61 (1-2), 93-125. doi: https://doi.org/10.1016/S0010-0277(96)00719-6

Soliva, R., Benedicto, A., Maerten, L., 2006. Spacing and linkage of confined normal faults: importance of mechanical thickness. J. Geophys. Res. Solid Earth. 111(B1), 1-17. doi: http://dx.doi.org/10.1029/2004JB003507

Walsh, J.J., Watterson, J., Bailey, W.R., Childs, C., 1999. Fault relays, bends and branch-lines. J. Struct. Geol. 21 (8-9), 1019-1026. doi: https://doi.org/10.1016/S0191-8141(99)00026-7

Torabi, A., Alaei, B., Libak, A., 2019. Normal fault 3D geometry and displacement revisited: Insights from faults in the Norwegian Barents Sea. Mar. Pet. Geol. 99,135-155. doi: https://doi.org/10.1016/j.marpetgeo.2018.09.032

Scott, D.H & Tanaka, K.L. 1986. Geologic map of the western equatorial region of Mars. U.S. Geol. Surv. Misc. Inv. Map 1-1802-A. doi: https://doi.org/10.3133/i1802A

Wise, D.U., Golombek, M.P., McGill, G.E., 1979. Tharsis Province of Mars: geologic sequence, geometry, and a deformation mechanism. Icarus 38, 456-472. doi: https://doi.org/10.1016/0019-1035(79)90200-8

Plescia, J.B & Saunders, R.S., 1982. Tectonic history of the Tharsis region. J. Geophys. Res. 87(12), 9775-979. doi: https://doi.org/10.1029/JB087iB12p09775

Plescia, J. B., 1991. Graben and extension in northern Tharsis, Mars. J. Geophys. Res. Planets. 96 (E3), 18883-18895. doi: https://doi.org/10.1029/91JE02005

Tanaka, K. L., Golombek, M. P. &Banerdt, W. B., 1991. Reconciliation of stress and structural histories of the Tharsis region of Mars. J. Geophys. Res. 96 (E1), 15617-15633. doi: https://doi.org/10.1029/91JE01194

Montgomery, D.R., Som, S.M., Jackson, M.P.A., Schreiber, B.C., Gillespie, A.R., Adams, J.B., 2009. Continental-scale salt tectonics on Mars and the origin of Valles Marineris and associated outflow channels. Geol. Soc. Am. Bull. 121 (1-2), 117-133. doi: https://doi.org/10.1130/B26307.1

Chavan, A., Sarkar, S., Bhandari, S., 2022. Episodic and declining fluvial processes in Noctis Fossae, Syria Planum Province, Mars. Adv. Space Res. 70, 3205-3219. doi: https://doi.org/10.1016/j.asr.2022.07.032

Fialko, Y. A., & Rubin, A.M.,1999. Thermal and mechanical aspects of magma emplacement in giant dike swarms. J. Geophys. Res.104 (B10), 23033-23049. doi: https://doi.org/10.1029/1999JB900213

Gudmundsson, A., 1990. Emplacement of dikes, sills and crustal magma chambers at divergent plate boundaries. Tectonophysics, 176 (3-4), 257-275. doi: https://doi.org/10.1016/0040-1951(90)90073-H

Gudmundsson, A., 2000. Fracture dimensions, displacements, and fluid transport. J. Struct. Geol. 22 (9), 1221-1231. doi: http://dx.doi.org/doi:10.1016/S0191-8141(00)00052-3

Gudmundsson, A., 2006. How local stresses control magma-chamber ruptures, dyke injections, and eruptions in composite volcanoes. Earth.Sci. Rev.79 (1-2),1-31. doi: https://doi.org/10.1016/j.earscirev.2006.06.006

Mège, D., Korme, T., 2004. Fissure eruption of flood basalts from statistical analysis of dyke fracture length. J. Volcanol. Geotherm. Res. 132 (1-2), 77-92. doi: http://dx.doi.org/10.1016/S0377-0273(03)00317-2

Chen, Z & Jin, Z.-H., 2006. Magma-driven subcritical crack growth and implications for dike initiation from a magma chamber. Geophys. Res. Lett.33 (19), L19307. doi: https://doi.org/10.1029/2006GL026979

Pozzobon, R., Mazzarini, F., Massironi, M., Marinangeli, L., 2014. Self-similar clustering distribution of structural features on Ascraeus Mons (Mars): implications for magma chamber depth. Geol. Soc. Spec. Publ. 401(1). doi: https://doi.org/10.1144/sp401.12

Okubo, C.H & Schultz, R.A., 2006.Variability in Early Amazonian Tharsis stress state based on wrinkle ridges and strike-slip faulting. J. Struct. Geol. 28 (12), 2169-2181. doi: https://doi.org/10.1016/j.jsg.2005.11.008